Tyrosine phosphorylation of mitofusin 2 regulates endoplasmic reticulum-mitochondria tethering

Peng Zhang[1,2,3#], Kara Ford[1,2], Jae Hwi Sung[4,5], Jacob Moeller[1], Yuta Suzuki[4], Iuliia Polina[4], Toshiaki Tachibana[6], Yoichiro Kusakari[7], Michael W Cypress[4], Isabel Chaput[4], Kamelia Drenkova[4], Maria Landherr[4], Stephanie M Adaniya[1,2,4], Jyotsna Mishra[8], Ulrike Mende[1,2], Bong Sook Jhun[4], Jin O-Uchi[4#]

[1]Cardiovascular Research Center, Lifespan Cardiovascular Institute, Rhode Island Hospital, Providence, Rhode Island, USA
[2]Department of Medicine, Division of Cardiology, Alpert Medical School of Brown University, Providence, Rhode Island, USA
[3]Vascular Research Laboratory, Providence VA Medical Center, Providence, Rhode Island, USA
[4]Lillehei Heart Institute, Department of Medicine, Cardiovascular Division, University of Minnesota, Minneapolis, MN, USA
[5]Department of Integrative Biology and Physiology, University of Minnesota Medical School, Minneapolis, MN, USA
[6]Core Research Facilities for Basic Science, Research Center for Medical Science, The Jikei University School of Medicine, Tokyo, Japan
[7]Center for Medical Education, The Jikei University School of Medicine, Tokyo, Japan
[8]Department of Anesthesiology, Medical College of Wisconsin, Milwaukee, Wisconsin, USA

 # Corresponding Authors

Peng Zhang, MD
Alpert Medical School of Brown University
Providence VA Medical Center/OSRI
Building 35, Room 231
830 Chalkstone Ave.
Providence, RI 02908
Tel: 401-273-7100 ext. 16321
Email: Peng_Zhang@brown.edu

Jin O-Uchi, MD, PhD
Lillehei Heart Institute, Cardiovascular Division, Department of Medicine
University of Minnesota
Cancer and Cardiovascular Research Building, Rm. 4-129
2231 6th St. SE, Minneapolis, MN 55455
Tel: 612-626-2521
Email: jouchi@umn.edu

Abstract

Contact sites between the mitochondria and endoplasmic reticulum (ER) are irregulates the exchange of lipids, Ca^{2+}, and reactive oxygen species (ROS) across the two organelles. Mitofusin 2 (Mfn2) has been shown as one of the major components tethering these two organelles. Several post-translational modifications (PTMs) of Mfn2 have been identified to modulate canonical (i.e., mitochondrial fusion) and non-canonical functions, such as mitophagy and activation of ER stress signaling, however there is little information whether any PTMs can regulate mitochondrial and ER tethering. Basal tyrosine phosphorylation of Mfn2 was detected by mass spectroscopy, but it is unknown whether Mfn2 is a substrate of mitochondria-localized tyrosine kinases. Here we show that the mitochondria-localized Src family tyrosine kinases including c-Src can phosphorylate Mfn2, which decreases distance between the mitochondria and ER, and increases Ca^{2+} transfer from the ER to mitochondria, followed by changes in ROS generation and mitochondrial bioenergetics. Our findings suggest that tyrosine phosphorylation of Mfn2 may uniquely work to fine-tune ER-mitochondrial Ca^{2+} transport under physiological conditions, without activating mitophagy or ER stress signaling.

Introduction

Mitochondria are cellular organelles that play multiple roles in the life and death of a cell, including ATP generation, reactive oxygen species (ROS) generation, cell apoptosis, and handling of the universal second messenger calcium (Ca^{2+}) [1, 2]. Because mitochondria are semi-autonomous organelles possessing their own unique DNA, proteins encoded by mitochondrial and nuclear DNA are integrated in the mitochondria to maintain and regulate mitochondrial function [1, 3]. Moreover, mitochondrial function may also be modulated through physical interactions with other organelles, such as the endoplasmic/sarcoplasmic reticulum (ER/SR), peroxisomes, and nucleus [1, 4].

Among these interactions between mitochondria and other organelles, the structural and functional importance of ER/SR and mitochondrial membranes, termed mitochondria-associated membranes (MAM), have been well recognized [5, 6]. MAM is involved in regulating lipid, Ca^{2+}, and ROS exchange across these two organelles, which is critical for the maintenance of mitochondrial bioenergetics [5, 6]. Recent studies reported that one of the major components of the tethering structure between the two organelles is mitofusin 2 (Mfn2), a dynamin-like GTPase associated with fusion of the outer mitochondrial membrane (OMM) [7, 8]. Indeed, Mfn2 ablation promotes not only the inhibition of its canonical function mitochondrial fusion, but also increases the distance between the ER and mitochondria, decreases agonist-evoked Ca^{2+} transfer from the ER to mitochondria, and alters bioenergetics [9, 10]. Based on knockout studies of Mfn2, it has been proposed that Mfn2 also serves as a key regulator of

mitophagy and ER stress signaling, which are currently recognized as the non-canonical roles of Mfn2 in addition to ER-mitochondria tethering [11-13].

Several post-translational modifications (PTMs) including serine/threonine phosphorylation and ubiquitination of Mfn2 have been identified that alter the fusion and mitophagy activity [8], but it is still unclear whether there are PTMs that regulate its tethering function. Data from mass spectroscopy reveals that there is basal tyrosine phosphorylation (P-Tyr) of Mfn2 (see online database PhosphoSitePlus) [14]. However, specific signaling pathways that regulate P-Tyr levels of Mfn2 are completely unknown. Non-receptor-type protein tyrosine kinases, including multiple Src family kinases (SFKs) and their negative regulator C-terminal Src kinase (CSK), have been observed in the mitochondria as well as the cytoplasm [15-17]. Among the eight members of the SFK family (Lyn, Hck, Lck, Blk, c-Src, Fyn, Yes, and Fgr) [18], four have been found in the mitochondria. Specifically, c-Src, Fyn, Lyn, and Fgr are detectable in the mitochondria by immunoblotting of the crude mitochondrial proteins and by immunogold-labeled transmitted electron microscopy (TEM) [15-17].

In this study, we show that Mfn2 is capable of being phosphorylated by SFKs including c-Src, and that increased phosphorylation of Mfn2 results in a decreased distance between the OMM and ER at contact sites, which leads to increased Ca^{2+} transfer from ER to mitochondria and ROS generation. This study provides a potential candidate for the cellular signaling involved in the fine tuning of the ER-mitochondria distance via PTM of Mfn2.

Results

Src family of protein kinases (SFKs) are capable of phosphorylating Mfn2

To test whether Mfn2 has the potential to be tyrosine phosphorylated (P-Tyr) by SFKs, we genetically increased SFK activity in HEK293T cells. First, we confirmed that SFK members c-Src, Lyn, and Fyn were detectable in the mitochondrial fraction of HEK293T cells (**Fig. 1A**), similar to a previous report from rat brain mitochondria [17]. In contrast, another previously reported mitochondria-localized SFK Fgr [17] was not observed in this cell line (**Fig. EV1**). Next, to activate SFKs, we generated a stable knock-down (KD) of CSK, a negative regulator of SFKs, by stably overexpressing shRNA targeting CSK or the empty vector PLKO.1 as a control (**Fig. 1B** and **Fig.EV2**). Relative to controls transfected with the empty vector PLKO.1, The expression levels of SFKs were not altered by CSK knockdown (CSK-KD) (**Fig S1**). To assess the activity of SFKs, total SFK autophosphorylation levels were detected by a specific antibody raised against a synthetic phosphopeptide corresponding to residues surrounding Tyr^{419} of human c-Src, which can cross-react with the autophosphorylation sites of all other SFKs [19]. In whole cell lysates, we found that SFK activity increased in CSK-KD cells compared to control (**Fig.1B and Fig. EV2**). Importantly, CSK-KD preferentially activates SFK activity in the mitochondria compared to the cytosol (**Fig. 1B**). Next, to test whether CSK-KD can modulate the P-Tyr levels of Mfn2, HA-tagged human Mfn2 was transiently expressed in CSK-KD cells and control cells, and P-Tyr levels in immunoprecipitated Mfn2 were detected by a general P-Tyr antibody. We found that CSK-KD significantly increased P-Tyr levels of Mfn2 (**Fig. 1C and D**). To further investigate which SFK member(s) found in the mitochondrial protein fraction [15-17] can phosphorylate Mfn2, we first overexpressed wild-type c-Src (c-Src-WT), a major SFK member, and its kinase-

inactive dominant-negative mutant c-Src-K295R (c-Src-DN) in HEK293T cells stably overexpressing human Mfn2-HA and assessed P-Tyr levels in immunoprecipitated Mfn2 (**Fig. 1E and F**). We found that P-Tyr levels of Mfn2 significantly increased after c-Src-WT overexpression (but not in c-Src-DN overexpression) compared to control cells (**Fig. 1F**). Using the same experimental system, we also determined that overexpression of the other mitochondrial localized SFK members Fyn, Lyn, and Fgr do not significantly alter P-Tyr of Mfn2 (**Fig. 1G and H**). Although the reported substrates of CSK are only SFK family, we also tested whether CSK can directly phosphorylate Mfn2. We found that CSK overexpression does not increase the P-Tyr levels in Mfn2 (**Fig. 1G and H**). Lastly, we used a series of proteinase K digestions on isolated mitochondria from HEK293T cells to differentially permeabilize the OMM and inner mitochondrial membranes (IMM) and assess the localization of c-Src. The mitochondria digestion assay revealed that that c-Src is abundant in the OMM, where Mfn2 is located, rather than in intra-mitochondrial space (**Fig. 1I and J**), indicating that c-Src located at the OMM is capable of phosphorylating Mfn2.

SKF activation increases ER-mitochondria interactions

Mfn2 has a key role in multiple mitochondrial and cellular functions (e.g., ER-mitochondria tethering, mitophagy, and ER stress) in addition to its canonical function as a mitochondrial fusion protein. The balance of these actions determines the mitochondrial shape, function, and distribution as well as the regulation of cell survival and death. Since we found that CSK-KD preferentially activates SFKs in the mitochondrial fraction (see **Fig. 1B**), we next explored the impact of P-Tyr of Mfn2 on these Mfn2 functions using CSK-KD cells. First, ER-mitochondria interactions were

assessed in live cells under confocal microscopy with a the Förster resonance energy transfer (FRET)-based assay using OMM-targeted monomeric CFP (mt-CFP) and ER membrane-targeted monomeric YFP (ER-YFP) as a donor and an acceptor, respectively (**Fig. 2A**). Expression of either mt-CFP or ER-YFP alone does not show a significant FRET signal in HEK293T cells; their co-expression is required (**Fig. 2B**). In HEK 293T cells with a stable knockdown of Mfn2 (Mfn2-KD), FRET between mt-CFP and ER-YFP was significantly lower than in control cells (**Fig. 2C-E**). Using this system, we found that FRET is significantly higher in CSK-KD cells compared to control cells (**Fig. 2F and G**), suggesting that the interaction between ER-mitochondria is enhanced in CSK-KD cells compared to control. We also biochemically confirmed that MAM increased in the CSK-KD cells compared to control by assessing the amount of ER membrane proteins IP_3 receptor isoform 1(IP_3R1) in the mitochondrial fraction (**Fig. EV3**). To further assess whether the increased ER-mitochondria interaction is mediated by SFK activity, we pre-incubated the cells with the SFK inhibitor PP2 (30 μM, 30 min). Pretreatment of PP2 for 30 min significantly decreased SFK activity in CSK-KD cells to control cells (**Fig. EV2**). In addition, PP2 was able to abolish the FRET observed increase in CSK-KD cells, indicating that these FRET changes are mediated via SFK activity (**Fig. 2H**). To further examine whether c-Src is involved in this mechanism, we genetically manipulated c-Src activity by overexpressing Src-WT and -DN (see also, **Fig. 1F**). We found that FRET increased after c-Src-WT but not c-Src-DN overexpression compared to control cells transfected with empty vector (**Fig. 2I**), indicating that increased FRET in CSK-KD cells is mainly caused by c-Src activation. Lastly, we showed that overexpression of Src-WT in Mfn2-KD does not increase FRET (**Fig. 2J**),

suggesting that the effect of c-Src on increased ER-mitochondria interactions is mediated via Mfn2.

To further investigate the ultrastructural alterations of ER-mitochondria contact sites by SFK activation, we assessed the ultrastructure of ER and mitochondria using TEM (**Fig. 3A**). Importantly, the averaged distance between ER membrane and OMM is significantly shorter in CSK-KD cells compared to control without a change in the average number of contact sites in each mitochondrion (i.e., number of associated ERs in each mitochondrion) or the morphology of mitochondrial cross-section (i.e., averaged aspect ratio [AR] of mitochondrial cross-section) (**Fig. 3B and C**). However, the ER–mitochondria interface length measured from each mitochondrial cross-section (**Fig. 3A and B**) was not altered by CSK-KD (**Fig. 3C**). These results indicate that SFK activation shortens the ER-mitochondria distance, possibly via c-Src-dependent Mfn2 phosphorylation, but does not significant alter the interface length or the number of contact sites for each mitochondrion.

SFK activation does not enhance mitochondrial fission/fusion, mitophagy, or ER stress

We next explored whether SFK activation influences other Mfn2 functions, such as enhancing mitochondrial fusion, mitophagy, and ER stress. First, changes in the mitochondrial morphology/networks were assessed by three parameters calculated from live cell imaging using confocal microscopy: 1) Form factor (FF), which indicates mitochondrial shape and networks; 2) AR, which indicates the ratio of major axis and minor axis; and 3) the size of the mitochondria (**Fig. 4A and B**). No significant difference was observed in mitochondrial shape and networks between control and

CSK-KD cells. In addition, there was no significant difference in the expression levels of major fission/fusion proteins including dynamin-related protein 1 (DRP1), mitochondrial fission factor (MFF), optic atrophy-1 (OPA1), Mitofusin 1 (Mfn1) and Mfn2, between CSK-KD and control cells (**Fig. EV1A/C**). These results indicate that SFK activity may not significantly affect mitochondrial fission/fusion activity. We next investigated whether SFK activity is involved in the mitochondrial quality control process (i.e., mitophagy) Autophagic flux assay in starved cells with a western blot of LC3. We found that there was no difference in the LC3-I/LC3-II ratio (**Fig. 4C)**. Moreover, we found that the numbers of mitophagosomes/autophagosomes in TEM images between CSK-KD and control cells were comparable (**Fig. 4D).** Lastly, we assessed whether ER stress increased by SFK activations via assessing the expression of ER stress markers including glucose-regulated protein 94 (Grp94), glucose-regulated protein 78 (Bip/Grp78), and C/EBP-homologous protein (CHOP) [11], Whereas we did not observe an increase in the levels of CHOP and Grp94 in CSK-KD cells, we observed a decrease in Grp78 (**Fig. 4E**). Together, these results indicate that P-Tyr of Mfn2 by SFKs preferentially impacts the ER-mitochondria tethering function of Mfn2 rather than its other major functions.

SFK activation facilitates ER-mitochondria Ca^{2+} transport

We next investigated whether SFK-mediated modification of the contact site impacts ER-to-mitochondria Ca^{2+} transport. To measure the changes in Ca^{2+} concentration at the mitochondrial matrix ($[Ca^{2+}]_{mt}$) in response to cytosolic Ca^{2+} elevation, we used the mitochondrial matrix-targeted Ca^{2+}-sensitive biosensor mtRCamp1h [20]. Specific localization of mtRCaMP1h in the mitochondria was confirmed in HEK293T cells co-

transfected with a mitochondria-matrix targeted GFP (mt-GFP) (**Fig. 5A**). To evoke cytosolic Ca^{2+} elevation in CSK-KD and control cells, IP_3R-mediated ER Ca^{2+} release was induced by ATP treatment which stimulates endogenous $G_{\alpha q/11}$ protein-coupled P2Y receptor and downstream IP_3 production [21]. We found that CSK-KD cells started to increase $[Ca^{2+}]_{mt}$ immediately after ATP stimulation, while the majority of control cells required over 5 sec more before they displayed $[Ca^{2+}]_{mt}$ elevation in response to ATP stimulation (**Fig. EV4**). In control cells, there are two distinct populations of cells which have either relatively fast- or slow-response to ATP (time-to-peak-$[Ca^{2+}]_{mt}$ ~15 sec or > 1 min, respectively). On the other hand, in CSK-KD cells, the time-to-peak-$[Ca^{2+}]_{mt}$ is normally distributed, and they did not contain a slow-response population (**Fig. EV4**). Along with the changes in the distribution of time to peak $[Ca^{2+}]_{mt}$ after CSK-KD, average time-to-peak-$[Ca^{2+}]_{mt}$ became significantly shorter in CSK-KD cells compared to control (**Fig. 5B and C**). In addition, $[Ca^{2+}]_{mt}$ elevation in response to ATP was significantly higher than control cells In CSK-KD cells, (**Fig. 5B and C**), although CSK-KD cells had a significantly more depolarized mitochondrial membrane potential ($\Delta\psi_m$) compared to control (**Fig. 5D and E**). Together, these results indicate that SFK activation changes the mitochondria Ca^{2+} uptake profile (increased peak $[Ca^{2+}]_{mt}$, faster response to cytosolic Ca^{2+} elevation, and faster mitochondrial Ca^{2+} uptake).

SFK activation modulates mitochondrial ROS

Our data clearly show that c-Src activation after CSK-KD increases the efficiency of ER-mitochondria Ca^{2+} transport, possibly by changing the distance between ER and mitochondria. Excessive mitochondrial Ca^{2+} uptake increases ROS production from mitochondria possibly via changing $\Delta\psi_m$ [22] and/or inhibiting complex I activity [23]. To

test if c-Src activation regulates mitochondrial ROS production, CSK-KD HEK293T cells were transfected with a mitochondrial matrix-targeted H_2O_2-sensitive biosensor mt-roGFP2-Orp1 [24] (**Fig. 6**). This pH-insensitive biosensor contains Orp-1, a peroxidase that catalyzes the oxidation from H_2O_2. When mt-roGFP2 and Orp-1 are coupled together, it creates a mitochondrial ROS-sensitive fluorescent biosensor. Increased mitochondrial ROS results in a decrease in mt-roGFP2-Orp1 fluorescence. We calculated the basal mitochondrial ROS levels and maximum mitochondrial ROS production by stimulating the cells with an oxidative stress inducer, tert-butyl hydroperoxide (T-BH) followed by the application of a reducing agent, dithiothreitol (DTT) using epi-fluorescent microscopy (**Fig. 6A**). We found that CSK-KD cells had a higher basal mitochondrial ROS level as well as higher maximum mitochondrial ROS production compared to control cells (**Fig. 6B**). Consistent with increased mitochondrial ROS and depolarized $\Delta\psi_m$, we observed reduced basal and maxmal respirations in CSK-KD cells compared to control (**Fig. 6C and D**). These results indicate that c-Src activation by CSK-KD modulates mitochondrial ROS and bioenergetics.

Discussion

In this study, we identified a novel mechanism that regulates ER-mitochondrial tethering, Ca^{2+} transport from the ER to mitochondria, and mitochondrial ROS production through P-Tyr of Mfn2 (**Fig. 7**). We found that one of the SFKs, c-Src, is located at the OMM where it phosphorylates Mfn2 tyrosine residue(s), which leads to a decreased distance of ER and OMM (**Figs. 2 and 3**). Moreover, SFK activation, likely via P-Tyr of Mfn2, enhances mitochondrial Ca^{2+} uptake (**Fig. 4**). These results provide

new insights into the molecular basis of the modulation of ER-mitochondria tethering machinery as well as mitochondrial Ca^{2+} handling at MAM. Furthermore, the results of this study unveil a new pathway that could be targeted for the development of novel drugs to protect against pathophysiological conditions resulting from mitochondrial Ca^{2+} overload.

Molecular mechanism underlying tyrosine phosphorylation of Mfn2

In this study, we show that SFK activation by knockdown of the SFK inhibitory protein CSK or c-Src overexpression significantly increases P-Tyr levels of Mfn2 (despite the difference of the magnitude of P-Tyr levels of Mfn2 depending on the experimental systems), indicating that c-Src-dependent Mfn2 phosphorylation is indispensable for regulating ER-mitochondria tethering. The mitochondrial localization of several SFK members including c-Src, Fyn, Lyn, and Fgr have been reported [15-17]. We confirmed that at least three family members (c-Src, Fyn, and Lyn) are detectable in the mitochondrial fractionation of HEK293T cells (**Fig. 1A**). Among these tyrosine kinases, the activity of c-Src in the mitochondria has been well-characterized. Ogura et al. reported that c-Src exists in all areas of the mitochondria (from OMM to mitochondrial matrix) in osteoclasts [16]. Our mitochondrial digestion assay suggests that c-Src is abundant in the OMM, where Mfn2 is located, rather than in the intramitochondrial space (**Fig. 1J**). These results support our notion that c-Src phosphorylates proteins at the OMM (i.e., Mfn2) in addition to the proteins at the mitochondrial matrix. Although we show that Fyn, Lyn, and Fgr are less likely to phosphorylate Mfn2 compared to c-Src (**Fig. 1H**), our results do not completely rule out the possibility that other SFKs and/or the downstream signaling of c-Src are capable of directly phosphorylating Mfn2 at the

OMM. Data from mass spectroscopy reveals several different types of PTMs in mouse or human Mfn2, including phosphorylation, ubiquitylation, acetylation, and methylation (see online database PhosphoSitePlus) [14]. Basal P-Tyr of Mfn2 at Y448 has been reported [25, 26], but neither its functional relevance nor its upstream signaling have been identified. Human Mfn2 contains 15 tyrosine residues: 10 in the N-terminus, 2 in the C-terminus, that are conserved across all eukaryotic species, and 3 tyrosine residues located in the transmembrane domains. Four tyrosine residues (Y61, Y81, and Y269 in the N-terminus, and Y752 in the C-terminus) are predicted to be potential c-Src phosphorylation sites, according to the phosphorylation prediction program GPS 2.0 [27]. Another program, Netphos 3.1, predicts only two sites (Y61 and Y269) [28]. Among these sites, only Y269 resides within the GTPase structure [8]. Future studies are needed to definitively determine the c-Src-specific phosphorylation site(s) in Mfn2.

Molecular mechanism underlying the regulation of ER-mitochondria tethering by tyrosine phosphorylation of Mfn2.

We found that knockdown of the SFK inhibitory protein CSK increases P-Tyr levels of Mfn2 and decreases the distance between ER and mitochondria without changing the interface length (**Fig. 3**). This is subsequently followed by increased Ca^{2+} transport between these two organelles (**Fig. 5**). We also found that CSK-KD does not cause major changes in mitochondrial morphology/network (**Fig. 4A and B**). The GTPase activity of Mfn2 is necessary for fusing the mitochondria as well as generating Mfn2-Mfn2 tethering units, as evidenced by functional assessments of Mfn2 knockout cells [9, 10] and in Mfn2 mutations found in Charcot-Marie-Tooth disease type 2A (CMT2A) [29]. In CMT2A, Mfn2 mutations found within its GTPase domain or its proximities cause

more severe neuropathy in patients compared to those with mutations located in other Mfn2 domains [30], and exhibit destruction of mitochondria-ER interactions via decreased Mfn2 GTPase activity [31]. In CMT2A patients, Mfn2 mutations found within its GTPase domain or its proximities cause more severe neuropathies [30] and destruction of mitochondria-ER interactions via decreased Mfn2 GTPase activity [31] compared to those with mutations located in other Mfn2 domains. Therefore, increased Mfn2 GTPase activity is expected to increase mitochondrial fusion and also to generate new tethering units, and to shorten the distance between two organelles. This idea is also supported by the previous reports from Csordas and his colleagues who expressed synthetic linkers to cultured cells [32]. They reported that increasing the number of linkers between ER and mitochondria can not only decrease the distance between ER and OMM, but also increase the interface length, followed by the enhancement of Ca^{2+} transport from ER to mitochondria [32, 33]. Therefore, P-Tyr of Mfn2 may not increase the number of tethering units (i.e., may not generate new tethering units), but more likely changes the length of existed tethering machinery, possibly via the conformation changes of its 3D structure. It has been shown that a ubiquitination of Mfn2 by E3 ubiquitin ligase Parkin at K416, which is located outside of GTPase domain, is required for maintaining OMM-ER distance without changing Mfn2 expression levels and its GTPase activity [34]. Therefore, it is possible that c-Src-specific phosphorylation site(s) may reside outside of the Mfn2 GTPase domain and may not directly alter its GTPase activity (similar to K416 ubiquitination), but instead alter the 3D structure of Mfn2. Indeed, we found that the majority of predicted c-Src-specific phosphorylation sites are outside of the GTPase domain (see previous section). Future studies will determine c-

Src-specific phosphorylation site(s) in Mfn2 and test the functional importance of these sites using non-phosphorylation and phosphorylation mimetic Mfn2 mutants.

Molecular mechanism underlying the regulation of ER-mitochondria Ca^{2+} transport by tyrosine phosphorylation of Mfn2

Our data suggest that SFK activation after CSK-KD or c-Src overexpression increases the efficiency of ER-to-mitochondria Ca^{2+} transport possibly via changes in the distance between ER and mitochondria (**Figs. 2. 3 and 7**). At the resting state, the electrochemical driving force for a mitochondrial Ca^{2+} uptake via the Ca^{2+} influx pathway MCU is provided by $\Delta\Psi_m$ across the IMM. Mitochondrial Ca^{2+} uptake rates are very slow near the resting cytosolic Ca^{2+} concentration ($[Ca^{2+}]_c$), but rapidly increase if the $[Ca^{2+}]_c$ in the proximity of mitochondria reaches around 10-20 μM [32, 35-37]. When IP_3R releases ER Ca^{2+} to the MAM, Ca^{2+} concentration at the microdomain ($[Ca^{2+}]_{MAM}$) exceeds 10 μM [32], which is sufficient to trigger mitochondrial Ca^{2+} uptake via MCU. Time-to-peak-$[Ca^{2+}]_{MAM}$ becomes shorter and peak $[Ca^{2+}]_{MAM}$ becomes larger when MAM space become smaller after decrease in the tethering length [32]. Indeed, despite mild (but significant) $\Delta\Psi_m$ depolarization in CSK-KD cells, we found that time-to-peak-$[Ca^{2+}]_m$ becomes shorter and peak $[Ca^{2+}]_m$ becomes larger compared to those in control cells, possibly in response the changes in $[Ca^{2+}]_{MAM}$. Therefore, our results support the notion that c-Src activation-dependent phosphorylation of Mfn2 is capable of changing the MAM space enough to impact the magnitude and the speed of changes in $[Ca^{2+}]_{MAM}$, and subsequently $[Ca^{2+}]_m$, in response to G_q protein-coupled receptor stimulation. However, we cannot completely exclude the possibility of other mechanisms being involved. For instance, SFK might change the profile of ER Ca^{2+} release, even

though we did not see any changes in IP_3R expression after CSK-KD (**Fig. EV3**). There are a few reports showing potential upregulation of ER Ca^{2+} release after c-Src activation with an unknown mechanism [38, 39]. Another potential mechanism that may be involved is decreased Ca^{2+} clearance speed in MAM space, although we did not observe any significant decrease in the expression of sarco/endoplasmic reticulum Ca^{2+}-ATPases after CSK-KD (data not shown). Nevertheless, the changes in $[Ca^{2+}]_m$ profile by CSK-KD are mainly derived from changes in MAM size, possibly the structural alteration of Mfn2 due to P-Tyr of Mfn2.

Role of SFK signaling in regulating mitochondrial functions

We found that CSK-KD increases P-Tyr levels of Mfn2 (**Fig. 1**) and modulates the MAM space size (**Fig. 3**), but we did not observe any significant impact to other major Mfn2 functions such as mitochondrial morphology, mitophagy or ER stress signaling. We also found changes in the profile of mitochondrial Ca^{2+} transport, $\Delta\Psi_m$, mitochondrial ROS, and mitochondrial respiration by SFK activation. Mitochondrial Ca^{2+} uptake rates are very slow near the resting $Ca^{2+}]_c$, but decreased MAM space may facilitate the increase in basal $[Ca^{2+}]_m$, followed by $\Delta\Psi_m$ depolarization, and increased mitochondrial ROS level [40]. Under well-coupled conditions, a stimulation of forward flow by itself would be expected to oxidize the electron transport chain (ETC) and thereby lower ROS levels [41]. Acceleration of electron flow within the ETC, however, may also oxidize NADH and NADPH, thereby depleting the anti-oxidative capacity [42]. Therefore, long-term changes in basal $[Ca^{2+}]_m$ by the decreased MAM space may decrease the amount of antioxidative capacity in the matrix, followed by an increase in ROS levels in mitochondria without a complete loss of $\Delta\Psi_m$. Although we found the majority of c-Src

located at the OMM rather than inside of mitochondria including matrix, c-Src itself [16] or its downstream tyrosine kinase families (e.g., Pyk2 [43]) inside the mitochondria may also participate in the mechanism underlying the changes in mitochondrial ROS and respiration activity. Several mitochondrial matrix proteins were proposed as a specific substrates of matrix-c-Src [15, 16, 44-47], and the phosphorylation of these proteins may modulate mitochondrial respiration. Due to different basal mitochondrial respiration rates and different expression levels of c-Src in the cell types used in each report, the overall impact of c-Src activation in the matrix on mitochondrial respiration is presently highly controversial (possibly), but several reports (e.g., [45]) showed that overexpression of mitochondria-matrix targeted c-Src does not affect mitochondrial ROS levels [45]. These reports suggest that the increased mitochondrial ROS observed in our experiments is likely not mediated via c-Src activation at the mitochondrial matrix, but more likely from other mitochondrial compartments such as c-Src at the OMM. However, a limitation of our current study is that the strategies of CSK-KD and c-Src overexpression modulate not only mitochondrial SFK activity, but also signaling from the non-mitochondrial compartments such as the plasma membrane. Future studies will be required to establish the genetic tools that can manipulate c-Src activity specifically at the OMM (e.g., OMM-targeted CSK or c-Src) and precisely dissect the impact of c-Src activity in each mitochondrial sub-compartment (i.e., OMM vs matrix) on mitochondrial functions.

In conclusion, our results demonstrate a molecular and functional role of c-Src-dependent P-Tyr of Mfn2 in ER-mitochondrial tethering, which clearly distinguishes its role from other PTMs of Mfn2. Tyrosine phosphorylation of Mfn2 may serve a unique

role in fine-tuning ER-mitochondrial Ca^{2+} transport under physiological conditions, without activating mitophagy or ER stress signaling. Elucidation of the unique biophysical characteristics and physiological functions of Mfn2 tyrosine phosphorylation is significant for understanding mitochondrial Ca^{2+} and ROS signaling in the regulation of cellular physiology and pathophysiology.

Material and Methods

Antibodies, Plasmids and Reagents

All antibodies used in this study are shown in **Appendix Table S1**. The plasmids used in this study are listed in **Appendix Table S2**. ER membrane-targeted monomeric yellow fluorescent protein (ER-YFP) was generated from ER membrane-targeted green fluorescent protein (ER-EGFP) (kindly provided by Dr. Tamas Balla, NIH/NICHD, Rockville, MD) [32] by replacing the GFP with monomeric YFP (mEYFP) [48].

All chemicals were purchased from Sigma-Aldrich (St. Louis, MO) except for: 2-mercaptoethanol (Bio-Rad, Hercules, CA); Proteinase K and dithiothreitol (DTT) (Gentrox, Shrewsberry, MA); Mito Tracker Deep Red and tetramethylrhodamine, ethyl ester (TMRE) (Thermo Fisher Scientific, , Waltham, MA); PP2 (Cayman Chemical, Ann Arbor, Michigan); Torin 1 (LC Laboratories, Woburn, MA); and thapsigargin (Alomone Labs, Jerusalem, Israel).

Cell Culture and Transient Transfection

HEK293T cells (kindly provided by Dr. Keigi Fujiwara (University Texas MD Anderson, Houston TX) and IP_3R1-null HEK293 cells (Kerafast, Inc., Boston, MA) [49] were maintained in Dulbecco's modified Eagle's medium (DMEM) (HyClone GE

Healthcare, Little Chalfont, UK) supplemented with 4.5 g/L glucose, 1 mM sodium pyruvate and 1% L-glutamine, 10% fetal bovine serum (GIBCO, Grand Island, NY, USA), 100 U/mL penicillin, 100 µg/mL streptomycin (Genesee Scientific, El Cajon, CA) at 37ºC with 5% CO_2 in a humidified incubator. For maintenance of stable cell lines, antibiotics [1.6 mg/mL of G418 (Corning, Corning, NY) or 0.5 mg/ml puromycin (Gemini Bio-Products, Sacramento, CA)] were added to the medium. Growth medium containing selection antibiotics was refreshed every 48 hrs [43, 50]. For transfection, cells were dissociated using Accutase (Innovative Cell Technologies, San Diego, CA) and plated on 3.5 or 10 cm dishes at 75-80% confluence one day before transfection. Cells were transfected with the plasmids (total 3 µg of plasmids in a 3.5-cm dish and 10 µg for a 10-cm dish) using FuGENE HD (Promega, Madison, WI) transfection reagent following the instruction provided by the manufacture. Twenty-four hours after transfection, cells were detached from the dish using Accutase and re-plated onto glass-bottom dishes (Matsunami USA, Bellingham, WA) or larger size dishes for subsequent live cell imaging, or biochemical experiments after additional 24-48 hours, respectively. For live-cell imaging, all culture medium was replaced by modified Tyrode's solution containing (136.9 mM NaCl, 5.4 mM KCl, 2 mM $CaCl_2$, 0.5 mM $MgCl_2$, 0.33 mM NaH_2PO_4, 5 mM HEPES, and 5 mM glucose. pH was adjusted to 7.4 using NaOH)[51].

Western Blot Analysis

Whole cell lysates from HEK293T cells were prepared with 1x lysis buffer (Cell Signaling Technology, Danvers, MA) containing protease inhibitor cocktail (Roche, Indianapolis, IN or Sigma Aldrich) and 1 mM phenylmethylsulfonyl fluoride (PMSF). Protein concentrations were determined by bicinchoninic acid (BCA) assay (Thermo

Fisher Scientific and G-Biosciences, St. Louis, MO). The samples were subjected to sodium dodecyl sulfate polyacrylamide (SDS)-PAGE and transferred to a nitrocellulose membrane for the near-infrared fluorescence immunoblotting. Membranes were blocked with blocking buffer (LI-COR Biotechnology, NE and Genesee Scientific, El Cajon, CA) and treated with primary antibodies followed by incubation with fluorescence-conjugated secondary antibodies (LI-COR Biotechnology). Odyssey infrared imaging system with Image Studio software (LI-COR Biotechnology). For Western blots performed by chemiluminescent immunoassay in Fig. 1B, membranes were blocked with 5% fat-free milk in PBS, probed with a primary antibody, followed by appropriate peroxidase-coupled secondary antibodies. The immunoreactive bands were visualized using SuperSignal West Pico or Femto reagents (Thermo Fisher Scientific). Quantitative densitometry was performed using ImageJ (NIH, available online at http://rsb.info.nih.gov/ij/).

Immunoprecipitation

Immunoprecipitations (IPs) were performed as we previously described [43, 51]. Briefly, whole cell lysates (500 µg) were incubated with primary antibodies (1-5 µg) overnight at 4°C. Protein A/G Plus Agarose (Santa Cruz) was added to the whole cell lysates for 2 hours at 4°C and the immunoprecipitates were collected by centrifugation at 1,000 g for 5 min at 4°C. After extensively washing the immunocomplexes with lysis buffer, 2x protein sample buffer was added to the immunocomplexes and the beads were dissociated by heating at 95°C for 5 min. The samples were subjected to Western blotting and immunoreactive bands were visualized by Odyssey infrared imaging system (LI-COR Biotechnology).

Protein Fractionation

Mitochondria-enriched and cytosolic fractions of HEK293T cells were obtained by protein fractionation using differential centrifugation [43, 50, 51]. Cells were collected from 150-mm dishes, resuspended in isolation buffer (320 mM sucrose, 1 mM EDTA, 10 mM Tris-HCl, pH 7.4) containing protease and phosphatase inhibitor cocktails (Roche, Indianapolis, IN or Sigma Aldrich). Cells were gently homogenized with a Dounce homogenizer. The mitochondrial and cytosolic proteins containing ER/SR proteins were separated by centrifugation at 17,000 x g for 15 min at 4°C. The mitochondrial-enriched fraction was re-suspended in lysis buffer containing 1 mM PMSF and protease inhibitor cocktail.

Mitochondrial Digestion Assay

Mitochondrial digestion was used to determine sub-mitochondrial localization of CSK as we previously described [43]. The mitochondrial-enriched pellet was re-suspended in 10 mM HEPES buffer (pH 7.2) with 280 mM sucrose and separated into eight samples (30 µg of the protein/tube) in 1.7 ml micro-centrifuge tubes. Each tube is treated with 100 µg/ml of proteinase K and differing percentages of digitonin (0.04% to 0.2%) for 15 min at room temperature. In addition to digitonin treatment, triton X-100 was used as a positive control to completely lyse the mitochondrial structure so that proteinase K can fully access all proteins. After proteinase K treatement, 10 mM of PMSF was added to each tube to stop the proteinase K digestion and Western blotting was performed. Proteins with known localization were immunoblotted and labeled according to their topology.

Quantitative Analyses of Mitochondrial Morphology

Mitochondria morphology was monitored in cells expressing mitochondrial matrix-targeted DsRed (mt-RFP) [52] using a laser scanning confocal microscope Olympus FV3000 (Olympus, Tokyo, Japan) at room temperature [50, 51]. Z-stack images of single HEK293T cells expressing mt-RFP were obtained, and single Z-projection images were created by Image J. Z-projection images were processed through a convolve filter of ImageJ software to obtain isolated and equalized fluorescent pixels. After converting the images, individual mitochondria were subjected to particle analysis to acquire values for circularity and aspect ratio (AR: major axis/minor axis) as previously described [50, 51]. The inverse of circularity was calculated to obtain form factor (FF). Increased AR values indicate long, tubular mitochondria, and increased FF values indicate increased mitochondrial branching and length. A value of 1 for both FF and AR indicates a perfect circle.

Quantitative Co-localization Analysis

The mitochondrial localization of GFP-tagged proteins was determined by co-expression with mitochondrial matrix-targeted marker mt-RFP based on co-localization [50]. Two-dimensional scatterplots of pixel intensities in green (GFP-tagged proteins) and red (mt-RFP) channels were generated with ImageJ software (NIH), and yellow color represents co-localized pixels. Co-localization of mt-RFP and GFP-tagged proteins in live cells was estimated using Pearson's correlation coefficient calculated via the Intensity Correlation Analysis plugin from ImageJ software (NIH) with the Intensity Correlation Analysis plug-in (Wright Cell Imaging Facility, Toronto Western Research Institute, Toroto, Canada), which examines the linear relationship between two

variables. The values for Pearson's correlation coefficient range from -1 to 1. A value of -1 represents a negative relationship; 0 represents no relationship; the value of 1 represents a positive relationship. Frequency and color scatter plots for each color channels were also created via ImageJ. Cells overexpressing both mt-GFP and mt-RFP were used as positive controls to show perfect co-localization and correlation.

Quantitative Analyses of Mitochondria/ER Membrane Interaction

Interaction between the OMM and ER membrane was assessed by the Förster resonance energy transfer (FRET) between OMM-targeted CFP (mt-CFP) and ER-mEYFP (see **Table 1**) using confocal microscopy (Olympus FV3000, Olympus) [51]. Briefly, HEK293T cells were co-transfected with equal amount of mt-CFP and ER-mEYFP. CFP and FRET images were sequentially acquired by the excitation wavelength of 405 nm, and emission wavelength of 475-488 nm and 535-560 nm, respectively. YFP images were obtained as a control (excitation at 488 nm and emission at 530-550 nm).

Transmitted Electron Microscopy (TEM)

ER-Mitochondrial interactions were assessed by transmission electron microscopy (TEM) as we previously reported (22, 24). HEK293T cells were fixed in 2.5% glutaraldehyde in 0.15 M Na cacodylate, 2% paraformaldehyde, and 2 mM $CaCl_2$ for 2-3 hours at 4°C, stained with uranyl acetate and lead aspartate, dehydrated in ethanol, and embedded in epoxy resin. Specimens were viewed with a TEM (JEM-1400Plus, JEOL, Tokyo, Japan) at 100 kV (26). Mitochondria size, number, and shape were assessed with ImageJ (NIH) (22, 24).

Measurement of Mitochondrial Ca^{2+} Uptake

The changes in mitochondrial matrix Ca^{2+} concentration ($[Ca^{2+}]_{mt}$) in response to the cytosolic Ca^{2+} elevation was measured in live cells transfected with a mitochondria-targeted Ca^{2+} biosensor mtRCaMP1h (kindly provided by Dr. Anita Aperia, Karolinska Institutet, Stockholm, Sweden) using a laser scanning confocal microscope Olympus FV3000 (Olympus) at room temperature [20]. Cells were plated on glass-bottom 35 mm dishes (Matsunami USA) for observation. Cell culture medium was replaced by modified Tyrode's solution containing 2 mM Ca^{2+} during observation. The mtRCaMp1h fluorescence was measured with excitation wavelength at 543 nm and emission wavelength at 560-660 nm every 5 sec. The mtRCaMp1h fluorescence (F) is converted into $\Delta F / F_0$, which shows the changes in $[Ca^{2+}]_{mt}$, where F_0 stands for initial fluorescence levels.

Measurement of Mitochondrial H_2O_2 Levels

A mitochondrial matrix-targeted H_2O_2-sensitive biosensor, mt-RoGFP2-Orp1 (gift from Dr. Tobias Dick, Deutsches Krebsforschungszentrum, Heidelberg, Germany), was used to measure H_2O_2 levels in live cell mitochondria [24]. HEK293T cells were transfected with mt-RoGFP2-Orp1 and used for experiments 48-72 hours after transfection. The fluorescence intensity from m t-RoGFP2-Orp1 (excitation and emission at 510 and 580 nm, respectively) was measured by an epifluorescence microscope equipped with 60× oil TIRF objective lens (Nikon, Tokyo, Japan) and Retiga EXi camera (QImaging, Surrey, BC, Canada) every 10 sec for 6 min [51]. To evaluate the capacity of maximal H_2O_2 production in the mitochondrial matrix, tert-butyl hydroperoxide (T-BH, 10 mM) was added to induce oxidative stress on the cells to stimulate maximum mitochondrial

H_2O_2 production. After cells reached maximal H_2O_2 production, 100 mM DTT was added as a reducing agent to assess the basal mitochondrial H_2O_2 level. The change in fluorescence intensity was calculated with ImageJ (NIH).

Measurement of Mitochondrial Membrane Potential

Mitochondrial membrane potentials ($\Delta\Psi_m$) were measured by $\Delta\Psi_m$-sensitive dye TMRE in live cells, along with $\Delta\Psi$-*insensitive* dye MitoTracker Deep Red [50]. Cells were incubated with 200 mM MitoTracker Deep Red and 500 mM TMRE for 15 minutes at 37 °C to stain the mitochondria and then washed with Tyrode solution. MitoTracker Deep Red fluorescence (excitation and emission at 644 and 665 nm, respectively) and TMRE fluorescence (excitation and emission at 540 and 580 nm, respectively) were simultaneously and time-dependently measured every 10 sec for 10 min with epifluorescence microscope (Nikon) and Retiga EXi camera (QImaging, Surrey). A mitochondrial oxidative phosphorylation un-coupler carbonyl cyanide m-chlorophenylhydrazone (CCCP, 10 μM) was added to cause $\Delta\Psi_m$ depolarization. TMRE intensity was calculated using the Intensity vs. Time monitor plugin from ImageJ software (NIH). The mitochondrial membrane potential was calculated after the addition of CCCP and normalized to the plateau region for each trace line.

Mitochondrial Respiration Measurement

Oxygen consumption rate (OCR) was measured with a Seahorse XFe96 Extracellular Flux analyzer (Agilent Technologies, Santa Clara, CA, USA) as we previously reported [51]. Briefly, HEK293T cells were seeded onto Seahorse XFe96 V3 PS cell culture microplates (Agilent Technologies) at a cell density of 30,000 cells per well and cultured overnight. The hydrated sensor cartridge was loaded in its injection ports with

oligomycin (1 μM), carbonyl cyanide-p-trifluoromethoxyphenylhydrazone (FCCP, 0.75 μM), and a mix of rotenone (1 μM) and antimycin A (1 μM), respectively. Seahorse XF DMEM medium (pH 7.4, Agilent Technologies) supplemented with 10 mM glucose, 1 mM pyruvate, and 2 mM L-glutamine was used as assay medium and replaced the culture medium 1 hr before assays. Measurements were taken for three cycles with 3 min mix and 3 min measurement per cycle following each injection. After completion of the assay, cells were stained with Hoechst 33342 (1 μg/ml, Thermo Fisher Scientific) for 30 min at room temperature protected from light, and fluorescent signals were measured with excitation/emission at 350/460 nm using a SynergyMx plate reader (BioTek Instruments, Winooski, VT) for cell number normalization.

Statistics

All data in the figures are shown as the mean ± standard error (SEM). Unpaired Student's t-test was performed, and a p-value of < 0.05 considered statistically significant. One-way ANOVA followed by Tukey's post-hoc test was used for multiple comparisons.

Acknowledgement

The work was supported by American Heart Association (AHA) 13SDG14370008 (to P.Z.), NIH/NIGMS 5P20GM103652 (Targeted project to P.Z.), NIH/NIGMS U54GM115677 (Targeted project to B.S.J.), AHA 18CDA34110091 (to B.S.J), NIH/NHLBI R01HL136757 (to J.O.-U.), NIH/NIGMS P30GM114750 (Pilot project to J.O.-U.), NIH/NIGMS P30GM110759 (Pilot project to J.O.-U.), AHA 16SDG27260248 (to J.O.-U.), American Physiological Society (APS) 2017 Shih-Chun Wang Young

Investigator Award (to J.O.-U.). The authors thank Ms. Michelle King, Ms. Amy K Landi, Dr. Xiaofei Li, Ms. Nedyalka Valkov, Ms. Gayathri Dileepan, and Ms. Dongqin Yang for their technical assistants.

Author contributions

P.Z. and J.O.-U. conceived and designed research; P.Z., K.F., J.H.S., Jacob.M., Y.S., I.P., T.T., Y.K., M.W.C., I.C., S.M.A., Jyotsna.M., B.S.J., and J.O.-U. performed experiments; P.Z., K.F., J.H.S., J.M., Y.S., I.P., K.D., M.L., B.S.J., and J.O.-U. analyzed data; P.Z, K.F., I.P., T.T., Y.K., M.W.C., Jacob.M U.M., B.S.J., and J.O.-U. interpreted results of experiments; P.Z., K.F., J.H.S., Y.S., B.S.J. and J.O.-U. prepared figures; J.O.-U. drafted manuscript; P.Z., I.P., M.W.C., Jacob.M., U.M., B.S.J., and J.O.-U. edited and revised manuscript; all authors approved final version of manuscript.

Conflict of interest

No conflicts of interest, financial or otherwise, are declared by the author(s).

Reference List

1. Rossmann MP, Dubois SM, Agarwal S, Zon LI (2021) Mitochondrial function in development and disease. Dis Model Mech **14:** 10.1242/dmm.048912. Epub 2021 Jun 11

2. Murphy E, Ardehali H, Balaban RS, DiLisa F, Dorn GW,2nd, Kitsis RN, Otsu K, Ping P, Rizzuto R, Sack MN et al. (2016) Mitochondrial Function, Biology, and Role in Disease: A Scientific Statement From the American Heart Association. Circ Res **118:** 1960-1991

3. Calvo SE, Mootha VK (2010) The mitochondrial proteome and human disease. Annu Rev Genomics Hum Genet **11:** 25-44

4. Xia M, Zhang Y, Jin K, Lu Z, Zeng Z, Xiong W (2019) Communication between mitochondria and other organelles: a brand-new perspective on mitochondria in cancer. Cell Biosci **9:** 27-019-0289-8. eCollection 2019

5. Barazzuol L, Giamogante F, Cali T (2021) Mitochondria Associated Membranes (MAMs): Architecture and physiopathological role. Cell Calcium **94:** 102343

6. Perrone M, Caroccia N, Genovese I, Missiroli S, Modesti L, Pedriali G, Vezzani B, Vitto VAM, Antenori M, Lebiedzinska-Arciszewska M et al. (2020) The role of mitochondria-associated membranes in cellular homeostasis and diseases. Int Rev Cell Mol Biol **350:** 119-196

7. Chandhok G, Lazarou M, Neumann B (2018) Structure, function, and regulation of mitofusin-2 in health and disease. Biol Rev Camb Philos Soc **93:** 933-949

8. Adaniya SM, O-Uchi J, Cypress MW, Kusakari Y, Jhun BS (2019) Post-Translational Modifications of Mitochondrial Fission and Fusion Proteins in Cardiac Physiology and Pathophysiology. Am J Physiol Cell Physiol

9. de Brito OM, Scorrano L (2008) Mitofusin 2 tethers endoplasmic reticulum to mitochondria. Nature **456:** 605-610

10. Naon D, Zaninello M, Giacomello M, Varanita T, Grespi F, Lakshminaranayan S, Serafini A, Semenzato M, Herkenne S, Hernandez-Alvarez MI et al. (2016) Critical reappraisal confirms that Mitofusin 2 is an endoplasmic reticulum-mitochondria tether. Proc Natl Acad Sci U S A **113:** 11249-11254

11. Ngoh GA, Papanicolaou KN, Walsh K (2012) Loss of mitofusin 2 promotes endoplasmic reticulum stress. J Biol Chem **287:** 20321-20332

12. Munoz JP, Ivanova S, Sanchez-Wandelmer J, Martinez-Cristobal P, Noguera E, Sancho A, Diaz-Ramos A, Hernandez-Alvarez MI, Sebastian D, Mauvezin C et al. (2013) Mfn2 modulates the UPR and mitochondrial function via repression of PERK. EMBO J **32:** 2348-2361

13. Sebastian D, Hernandez-Alvarez MI, Segales J, Sorianello E, Munoz JP, Sala D, Waget A, Liesa M, Paz JC, Gopalacharyulu P et al. (2012) Mitofusin 2 (Mfn2) links mitochondrial and endoplasmic reticulum function with insulin signaling and is essential for normal glucose homeostasis. Proc Natl Acad Sci U S A **109:** 5523-5528

14. Hornbeck PV, Zhang B, Murray B, Kornhauser JM, Latham V, Skrzypek E (2015) PhosphoSitePlus, 2014: mutations, PTMs and recalibrations. Nucleic Acids Res **43:** D512-20

15. Miyazaki T, Tanaka S, Sanjay A, Baron R (2006) The role of c-Src kinase in the regulation of osteoclast function. Mod Rheumatol **16:** 68-74

16. Miyazaki T, Neff L, Tanaka S, Horne WC, Baron R (2003) Regulation of cytochrome c oxidase activity by c-Src in osteoclasts. J Cell Biol **160:** 709-718

17. Tibaldi E, Brunati AM, Massimino ML, Stringaro A, Colone M, Agostinelli E, Arancia G, Toninello A (2008) Src-Tyrosine kinases are major agents in mitochondrial tyrosine phosphorylation. J Cell Biochem **104:** 840-849

18. Okada M (2012) Regulation of the SRC family kinases by Csk. Int J Biol Sci **8:** 1385-1397

19. Du G, Wang J, Zhang T, Ding Q, Jia X, Zhao X, Dong J, Yang X, Lu S, Zhang C et al. (2020) Targeting Src family kinase member Fyn by Saracatinib attenuated liver fibrosis in vitro and in vivo. Cell Death Dis **11:** 118-020-2229-2

20. Hamilton S, Terentyeva R, Kim TY, Bronk P, Clements RT, O-Uchi J, Csordas G, Choi BR, Terentyev D (2018) Pharmacological Modulation of Mitochondrial Ca(2+) Content Regulates Sarcoplasmic Reticulum Ca(2+) Release via Oxidation of the Ryanodine Receptor by Mitochondria-Derived Reactive Oxygen Species. Front Physiol **9:** 1831

21. Schrage R, Schmitz AL, Gaffal E, Annala S, Kehraus S, Wenzel D, Bullesbach KM, Bald T, Inoue A, Shinjo Y et al. (2015) The experimental power of FR900359 to study Gq-regulated biological processes. Nat Commun **6:** 10156

22. Jhun BS, Mishra J, Monaco S, Fu D, Jiang W, Sheu SS, O-Uchi J (2016) The mitochondrial Ca2+ uniporter: Regulation by auxiliary subunits and signal transduction pathways. Am J Physiol Cell Physiol **311(1):** C67-C80

23. Malyala S, Zhang Y, Strubbe JO, Bazil JN (2019) Calcium phosphate precipitation inhibits mitochondrial energy metabolism. PLoS Comput Biol **15:** e1006719

24. Meyer AJ, Dick TP (2010) Fluorescent protein-based redox probes. Antioxid Redox Signal **13:** 621-650

25. Drake JM, Graham NA, Stoyanova T, Sedghi A, Goldstein AS, Cai H, Smith DA, Zhang H, Komisopoulou E, Huang J et al. (2012) Oncogene-specific activation of tyrosine kinase networks during prostate cancer progression. Proc Natl Acad Sci U S A **109:** 1643-1648

26. Huttlin EL, Jedrychowski MP, Elias JE, Goswami T, Rad R, Beausoleil SA, Villen J, Haas W, Sowa ME, Gygi SP (2010) A tissue-specific atlas of mouse protein phosphorylation and expression. Cell **143:** 1174-1189

27. Xue Y, Ren J, Gao X, Jin C, Wen L, Yao X (2008) GPS 2.0, a tool to predict kinase-specific phosphorylation sites in hierarchy. Mol Cell Proteomics **7:** 1598-1608

28. Blom N, Gammeltoft S, Brunak S (1999) Sequence and structure-based prediction of eukaryotic protein phosphorylation sites. J Mol Biol **294:** 1351-1362

29. Zuchner S, Mersiyanova IV, Muglia M, Bissar-Tadmouri N, Rochelle J, Dadali EL, Zappia M, Nelis E, Patitucci A, Senderek J et al. (2004) Mutations in the mitochondrial GTPase mitofusin 2 cause Charcot-Marie-Tooth neuropathy type 2A. Nat Genet **36:** 449-451

30. Stuppia G, Rizzo F, Riboldi G, Del Bo R, Nizzardo M, Simone C, Comi GP, Bresolin N, Corti S (2015) MFN2-related neuropathies: Clinical features, molecular pathogenesis and therapeutic perspectives. J Neurol Sci **356:** 7-18

31. Larrea D, Pera M, Gonnelli A, Quintana-Cabrera R, Akman HO, Guardia-Laguarta C, Velasco KR, Area-Gomez E, Dal Bello F, De Stefani D et al. (2019) MFN2 mutations in Charcot-Marie-Tooth disease alter mitochondria-associated ER membrane function but do not impair bioenergetics. Hum Mol Genet **28:** 1782-1800

32. Csordas G, Varnai P, Golenar T, Roy S, Purkins G, Schneider TG, Balla T, Hajnoczky G (2010) Imaging interorganelle contacts and local calcium dynamics at the ER-mitochondrial interface. Mol Cell **39:** 121-132

33. Garcia-Perez C, Schneider TG, Hajnoczky G, Csordas G (2011) Alignment of sarcoplasmic reticulum-mitochondrial junctions with mitochondrial contact points. Am J Physiol Heart Circ Physiol **301:** H1907-15

34. Basso V, Marchesan E, Peggion C, Chakraborty J, von Stockum S, Giacomello M, Ottolini D, Debattisti V, Caicci F, Tasca E et al. (2018) Regulation of ER-mitochondria contacts by Parkin via Mfn2. Pharmacol Res **138:** 43-56

35. Csordas G, Thomas AP, Hajnoczky G (1999) Quasi-synaptic calcium signal transmission between endoplasmic reticulum and mitochondria. EMBO J **18:** 96-108

36. Rizzuto R, Pinton P, Carrington W, Fay FS, Fogarty KE, Lifshitz LM, Tuft RA, Pozzan T (1998) Close contacts with the endoplasmic reticulum as determinants of mitochondrial Ca2+ responses. Science **280:** 1763-1766

37. Giacomello M, Drago I, Bortolozzi M, Scorzeto M, Gianelle A, Pizzo P, Pozzan T (2010) Ca2+ hot spots on the mitochondrial surface are generated by Ca2+ mobilization from stores, but not by activation of store-operated Ca2+ channels. Mol Cell **38:** 280-290

38. Aziz AUR, Geng C, Li W, Yu X, Qin KR, Wang H, Liu B (2019) Doxorubicin Induces ER Calcium Release via Src in Rat Ovarian Follicles. Toxicol Sci **168:** 171-178

39. Tokmakov AA, Sato KI, Iwasaki T, Fukami Y (2002) Src kinase induces calcium release in Xenopus egg extracts via PLCgamma and IP3-dependent mechanism. Cell Calcium **32:** 11-20

40. Cao JL, Adaniya SM, Cypress MW, Suzuki Y, Kusakari Y, Jhun BS, O-Uchi J (2019) Role of mitochondrial Ca(2+) homeostasis in cardiac muscles. Arch Biochem Biophys **663:** 276-287

41. Nicholls DG (2004) Mitochondrial membrane potential and aging. Aging Cell **3:** 35-40

42. Aon MA, Cortassa S, O'Rourke B (2010) Redox-optimized ROS balance: a unifying hypothesis. Biochim Biophys Acta **1797:** 865-877

43. O-Uchi J, Jhun BS, Xu S, Hurst S, Raffaello A, Liu X, Yi B, Zhang H, Gross P, Mishra J et al. (2014) Adrenergic signaling regulates mitochondrial Ca2+ uptake through Pyk2-dependent tyrosine phosphorylation of the mitochondrial Ca2+ uniporter. Antioxid Redox Signal **21:** 863-879

44. Ogura M, Yamaki J, Homma MK, Homma Y (2012) Mitochondrial c-Src regulates cell survival through phosphorylation of respiratory chain components. Biochem J **447:** 281-289

45. Ogura M, Yamaki J, Homma MK, Homma Y (2014) Phosphorylation of flotillin-1 by mitochondrial c-Src is required to prevent the production of reactive oxygen species. FEBS Lett **588:** 2837-2843

46. Djeungoue-Petga MA, Lurette O, Jean S, Hamel-Cote G, Martin-Jimenez R, Bou M, Cannich A, Roy P, Hebert-Chatelain E (2019) Intramitochondrial Src kinase links mitochondrial dysfunctions and aggressiveness of breast cancer cells. Cell Death Dis **10:** 940-019-2134-8

47. Hebert-Chatelain E, Jose C, Gutierrez Cortes N, Dupuy JW, Rocher C, Dachary-Prigent J, Letellier T (2012) Preservation of NADH ubiquinone-oxidoreductase activity by Src kinase-mediated phosphorylation of NDUFB10. Biochim Biophys Acta **1817:** 718-725

48. Zacharias DA, Violin JD, Newton AC, Tsien RY (2002) Partitioning of lipid-modified monomeric GFPs into membrane microdomains of live cells. Science **296:** 913-916

49. Alzayady KJ, Wang L, Chandrasekhar R, Wagner LE,2nd, Van Petegem F, Yule DI (2016) Defining the stoichiometry of inositol 1,4,5-trisphosphate binding required to initiate Ca2+ release. Sci Signal **9:** ra35

50. O-Uchi J, Jhun BS, Hurst S, Bisetto S, Gross P, Chen M, Kettlewell S, Park J, Oyamada H, Smith GL et al. (2013) Overexpression of ryanodine receptor type 1

enhances mitochondrial fragmentation and Ca2+-induced ATP production in cardiac H9c2 myoblasts. Am J Physiol Heart Circ Physiol

51. Jhun BS, O-Uchi J, Adaniya SM, Mancini TJ, Cao JL, King ME, Landi AK, Ma H, Shin M, Yang D et al. (2018) Protein kinase D activation induces mitochondrial fragmentation and dysfunction in cardiomyocytes. J Physiol **596:** 827-855

52. Yoon Y, Krueger EW, Oswald BJ, McNiven MA (2003) The mitochondrial protein hFis1 regulates mitochondrial fission in mammalian cells through an interaction with the dynamin-like protein DLP1. Mol Cell Biol **23:** 5409-5420

53. Yamada Y, Kusakari Y, Akaoka M, Watanabe M, Tanihata J, Nishioka N, Bochimoto H, Akaike T, Tachibana T, Minamisawa S (2021) Thiamine treatment preserves cardiac function against ischemia injury via maintaining mitochondrial size and ATP levels. J Appl Physiol (1985) **130:** 26-35

Figure legends

Fig. 1. SFK phosphorylates Mfn2

A. Expression of SFK members after mitochondrial fractionation of HEK293T cells. Argonaute 2 (Argo2) was used as a marker for the cytosolic fraction (Cyto). Voltage-dependent anion channel (VDAC), cytochrome c oxidase subunit 4 (COX4), and optic atrophy-1 (OPA1) were used as markers for the mitochondrial fraction (Mito). WCL, whole cell lysates. Representative images from 3 independent experiments. **B.** CSK-KD increases SFK activity in mitochondria. Representative immunoblotting images from HEK293T cells stably overexpressing CSK-shRNA (CSK-KD cells). Control cells (CTR) were prepared by overexpression of PLKO.1 empty vector. Immunoreactive bands were visualized by chemiluminescent immunoassay. Argo2 was used as a marker for the Cyto. VDAC, and COX4 were used as markers for the Mito. Glyceraldehyde 3-phosphate dehydrogenase (GAPDH) was used for loading control for the WCL. IP, immunoprecipitation. IB, immunoblotting. **C.** Increased P-Tyr of Mfn2 in HEK293T cells

by CSK knockdown. CTR and CSK-KD cells were transiently transfected with either Mfn2-HA or empty vector. Immunoprecipitation (IP) was performed with HA antibody, and P-Tyr of Mfn2 was detected by a general P-Tyr antibody. **D.** Summary data of C (n=4). Band intensity of immunoprecipitated P-Tyr was normalized to Mfn2. * p<0.05. **E.** Overexpression of c-Src increases P-Tyr of Mfn2. HEK293T cells stably overexpressing Mfn2-HA was transiently transfected with either empty vector (pcDNA3.1(+) as a control), c-Src-WT, or c-Src-DN. IP was performed with HA antibody, and P-Tyr of Mfn2 was detected by a general P-Tyr antibody. Band intensity of immunoprecipitated P-Tyr was normalized to Mfn2. **F.** Summary data of E (n=4). * p<0.05. **G.** Overexpression of c-Src, but not other SFK members increases P-Tyr of Mfn2. HEK293T cells stably overexpressing Mfn2-HA were transiently transfected with either empty vector (pWZL-Neo-Myr-Flag-DEST as a control), c-Src, CSK, Fyn, Lyn, or Fgr. IP was performed with HA antibody, and P-Tyr of Mfn2 was detected by a general P-Tyr antibody. **H.** Summary data of G (n=9). Band intensity of the immunoprecipitated P-Tyr band was normalized by that in HA. * p<0.05. **I.** Submitochondrial localizations of marker proteins for mitochondria digestion assay. Red dots indicate the antibody binding sites. IMM, inner mitochondrial membrane; IMS, intermembrane space of mitochondria; Omi, human HTRA2; CyD cyclophilin D. **J.** Representative immunoblotting pattern of mitochondria digestion for umtiochodrial localization of c-Src. PK, Proteinase K; Dig, digitonin.

Fig. 2. SFK activation enhances ER-mitochondria interaction

A. Schematic diagram of a FRET donor and acceptor for assessing ER-mitochondria interaction. TMD, trans membrane domain. **B.** Expression of FRET sensors in HEK293T

cells. Representative images of FRET detection in HEK293T cells transiently transfected with mt-CFP, ER-YFP, or both constructs. Scale bar, 20 μm. **C.** *(Top):* Representative near-infrared fluorescence immunoblotting of whole cell lysates obtained from HEK293T stably overexpressing Mfn2-shRNA (Mfn2-KD) or PLKO.1 (control; CTR). IP, immunoprecipitation. IB, immunoblotting. *(Bottom):* Summary data (n=3). Mfn2 band intensity was normalized by that in tubulin. * p<0.05. **D.** Mfn2 knockdown decreases ER-mitochondria interaction. Representative images of FRET detection in Mfn2-KD or CTR cells transfected with mt-CFP and ER-YFP. Scale bar, 20 μm. **E.** Summary of normalized FRET/CFP ratio from panel D (n=104 and 100, for CTR and Mfn2-KD, respectively). *p<0.05. **F.** CSK knockdown decreases ER-mitochondria interaction. Representative images of FRET detection in CSK-KD or CTR cells transfected with mt-CFP and ER-YFP. Scale bar, 20 μm. **G.** Summary of normalized FRET/CFP ratio from panel E (n=132 and 135, for CTR and Mfn2-KD, respectively). *p<0.05. **H**. Effect of a SFK inhibitor PP2 on FRET/CFP ratio. CSK-KD or CTR HEK293T cells were co-transfected with FRET biosensors and treated with PP2 (30 μM) or DMSO (vehicle) for 30 min before FRET measurements (n=58, 50, 54, and 26 for CTR+DMSO, CTR+PP2, CSK-KD+DMSO, and CSK-KD+PP2, respectively). *p<0.05. **I.** Effect of a c-Src on FRET/CFP ratio. c-Src-WT, c-Src-DN, or pWZL empty vector (as a control) were co-transfected with FRET biosensors into HEK293T cells. (n=110, 117, and 118 for CTR, c-Src-WT and c-Src-DN respectively). * p<0.05. **J.** Effect of a c-Src on FRET/CFP ratio in Mfn2-KD cells. c-Src-WT, or pWZL (as a control) were co-transfected with FRET biosensors into HEK293T cells. (n=110, 117, and 118 for CTR, c-Src-WT and c-Src-DN respectively). * p<0.05.

Fig. 3. SFK activation shortens a distance between ER and mitochondria

A. Representative images of transmission electron microscopy (TEM) in HEK293T cells. White lines, green lines, yellow area, and blue area represent OMM, MAM interface, ER area, and mitophagosome area, respectively. MAM distances from three points (Red lines) were averaged to estimate the distance between ER and OMM. Scale bars, 500 nm. **B.** Representative TEM images in CSK-KD and CTR HEK293T cells. Scale bar, 500 nm. Arrows point to the ER and mitochondria interaction sites. **C.** Summary data from B. Number in parentheses indicates the total number of images analyzed in each group * $p<0.05$.

Fig. 4. **SFK activation does not enhance mitochondrial fusion, mitophagy, or ER stress signaling.**

A. Summary data of mitochondrial size, form factor (FF), and AR in CTR and CSK-KD HEK293T cells (n=4249 and 4394, respectively). Cells were transfected with matrix-targeted DsRed (mt-RFP), and analyzed with live cell imaging using confocal microscopy. N.S., not significant. **B.** Comparison of AR and FF of individual mitochondria in CSK-KD cells vs. CTR cells. **C.** *(Top)***:** Representative immunoblotting of LC3-I/LC3-II obtained from CTR and CSK-KD HEK293T cells. Lysates from HEK293T cells treated with Torin1 are shown as a positive control that changes LC3-I/LC3-II ratio. *(Bottom):* Summary data for LC3-1/LC3-II ratio (n=4). **D.** Mitophagosome number counted from TEM images of CTR and CSK-KD HEK293T cells (n=60, and 83,

respectively) (see also Fig. 3). **E.** SFK activation does not promote ER stress. *(Top):* Immunoblotting of ER stress markers, Grp94, Grp78, and CHOP obtained from CTR and CSK-KD HEK293T cells. Lysates from HEK293T cells treated with thapsigargin (TG) were shown as a positive control that increases ER stress. *(Bottom):* Summary data (*n*=4). Grp94 and Grp78 band intensities were normalized to tubulin. * *p*<0.05.

Fig. 5. SFK activation increases mitochondrial Ca^{2+} uptake in response to cytosolic Ca^{2+} elevation

A. Expression of mitochondria-targeted Ca^{2+}-sensitive biosensor, mt-RCaMP1h, in HEK293T cells co-transfected with mitochondrial matrix-targeted GFP (mt-GFP). **B.** Representative traces of changes in Ca^{2+} concentration in the mitochondrial matrix ($[Ca^{2+}]_m$) uptake trace in CTR or CSK-KD HEK293T cells in response to $G_{\alpha q/11}$ protein-coupled P2Y receptor stimulation by 1 mM ATP. $[Ca^{2+}]_m$ was assessed by mt-RCamp1h. **C.** Summary data of B (*n*=36 and n=56 for CTR and CSK-KD cells, respectively). * p<0.05. **D.** Averaged traces of the changes in the fluorescence intensity of tetramethylrhodamine, ethyl ester (TMRE) in response to the treatment with CCCP in CTR and CSK-KD HEK293T cells. Initial TMRE intensity before CCCP treatment was normalized with the value after CCCP treatment. **E.** Summary data of A (*n*=50 and n=65 for CTR and CSK-KD cells, respectively). **p*<0.05

Fig. 6. SFK activation increases mitochondrial ROS

A. Representative time-lapse images (top) and traces (bottom) of HEK293T cells transfected with mitochondrial targeted ro-GFP2-Orp1 (mt-roGFP2-Orp1) upon

stimulation with an oxidative stress inducer, tert-butyl hydroperoxide (T-BH, 10 mM) and a reducing agent, dithiothreitol (DTT, 100 mM). **B.** Summary data of A (*n*=32, and 22 for CTR and CSK-KD cells, respectively). **p*<0.05. **C.** Oxygen consumption rate (OCR) measurements obtained over time (min) using an extracellular flux analyzer in CTR and CSK-KD cells. Data from 3 independent experiments. **D.** Summary data of C (*n*=3 for each group). **p*<0.05.

Fig. 7. Tyrosine phosphorylation of Mfn2 regulates ER-mitochondria tethering

One of the SFKs, c-Src, is located at the OMM and capable of phosphorylating Mfn2 tyrosine residue(s), which leads to a decreased distance of ER and OMM, possibly via the conformation changes of its 3D structure. The decreased distance of ER and OMM enhances Ca^{2+} transport from ER to Mitochondria, followed by the increased in mitochondrial ROS. MCU, mitochondrial Ca^{2+} uniporter; NCX, mitochondrial Na^{+}/Ca^{2+} exchanger; mPTP, mitochondrial permeability transition pore.

Expanded View Figure legends

Fig. EV1. Expression levels of Src family and mitochondrial fission/fusion proteins are not altered by CSK knockdown

A. Representative immunoblots of whole cell lysates obtained from different passages of HEK293T cells stably overexpressing PLKO.1 (control, CTR) or CSK- shRNA (CSK-KD). A lysate of HEK293T cells overexpressing Fgr was used as a positive control for Fgr. Mfn1, Mitofusin 1; Mff, mitochondrial fission factor; Opa1, optic atrophy-1; DRP1, dynamin-related protein 1. **B.** Summary data of SFK expression levels. Each band intensity was normalized by tubulin (n=4 for each group). * p<0.05. N.S., not significant. **C.** Summary data of mitochondrial fission/fusion protein expression levels (n=4 for each group). Each band intensity was normalized by tubulin. * p<0.05. N.S., not significant.

Fig. EV2. Concentration-dependent effect of PP2 on Src family activity in CSK-knock down and control cells

A. Representative near-infrared fluorescence immunoblotting of whole cell lysates obtained from HEK293T cells stably overexpressing PLKO.1 (control, CTR) or CSK-shRNA (CSK-KD) that were treated with the SFK inhibitor PP2 for 30 min. **B.** Summary data of panel A (CSK-KD in red, CTR in black). Band intensity was normalized by GAPDH (n=4 for each group). * p<0.05, compared to CTR at each PP2 concentration.

Fig. EV3. SFK activation increases a MAM protein IP3 receptor

A. Representative immunoblotting of whole cell lysates obtained from HEK293T cells and IP_3 receptor isoform 1 (IP_3R-1) knockout HEK293 cell line. IP_3R-1 was detected by a specific antibody against rat IP_3R-1. **B.** Immunoblotting of IP_3R-1 in whole cell lysates obtained from HEK293T cells stably overexpressing CSK-shRNA (CSK-KD) or PLKO.1 (control; CTR). **C.** Summary data of B. IP_3R-1 band intensities were normalized by tubulin (*n*=4). N.S., not significant. **D.** Protein fractionations from CSK-KD and CTR cells. IP_3R-1 was used to assess the MAM protein amount in the mitochondrial fraction. Mito, mitochondrial fraction; Cyto, cytosolic fraction including ER and plasma membrane; WCL, whole cell lysate. **E.** Summary data of the IP_3R-1 expression ratio between Mito and Cyto (*n*=4). IP_3R-1 expression levels in Mito and Cyto in each cell line were compensated by the amount of COX4 and Argo2, respectively, before calculating the Mito/Cyto ratio. * $p<0.05$.

Fig. EV4. SFK activation increases the time-to-peak-mitochondrial Ca^{2+} concentration in response to cytosolic Ca^{2+} elevation

A. Traces of the changes in Ca^{2+} concentration in mitochondrial matrix ($[Ca^{2+}]_m$) uptake obtained from individual HEK293T cells stably overexpressing PLKO.1 (control: CTR) or CSK-shRNA (CSK knockdown: CSK-KD) in response to $G_{\alpha q/11}$ protein-coupled P2Y receptor stimulation by 1 mM ATP. $[Ca^{2+}]_m$ was assessed with the mitochondrial matrix-targeted Ca^{2+} biosensor mt-RCamp1h (*n*=36 and n=56 for CTR and CSK-KD cells, respectively). **B.** Summary data of A. Black and red bars are from CTR and CSK-KD cells, respectively.

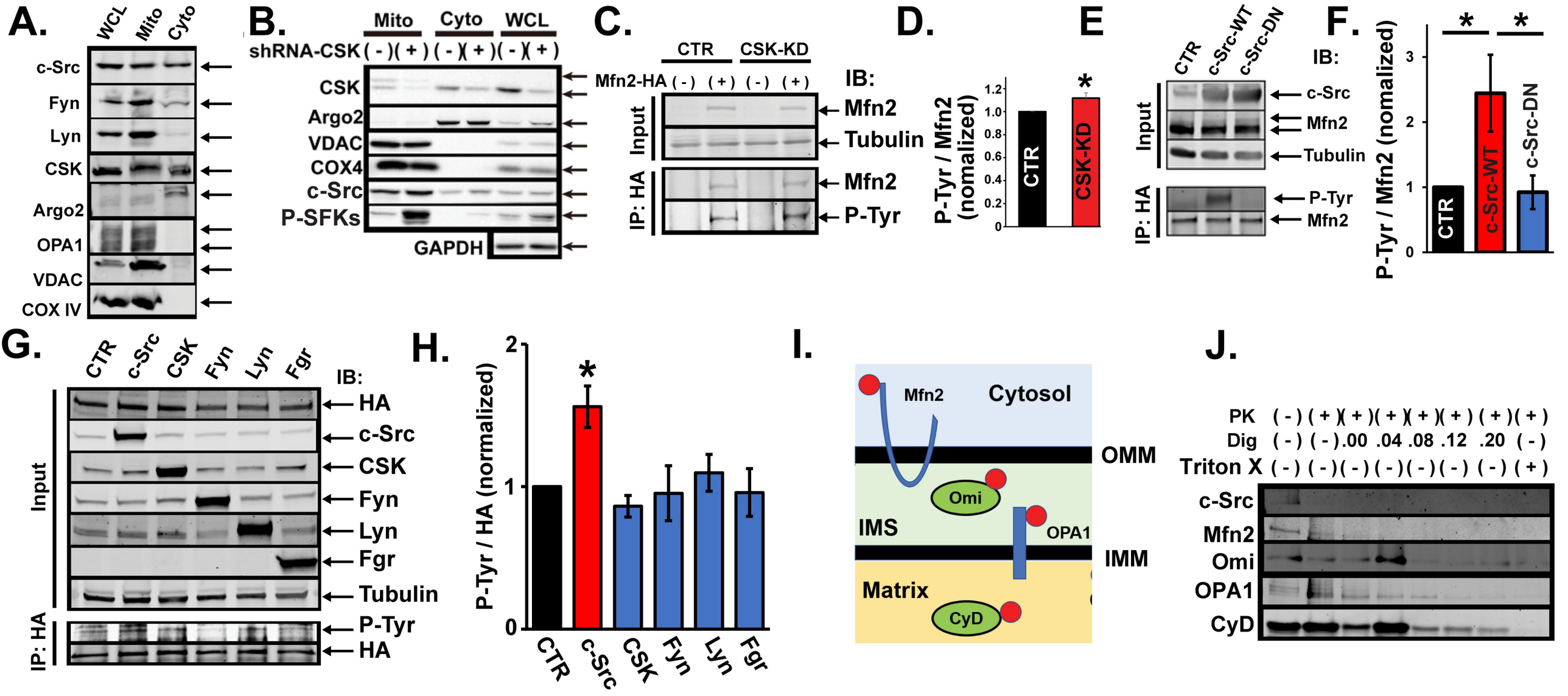
A.
WCL
Mito
Cyto
c-Src
Fyn
Lyn
CSK
Argo2
OPA1
VDAC
COX IV
B.
Mito
Cyto
WCL
shRNA-CSK (-)(+) (-)(+)(-)(+)
CSK
Argo2
VDAC
COX4
c-Src
P-SFKs
GAPDH
C.
CTR
CSK-KD
Mfn2-HA (-) (+) (-) (+)
IB:
Input
Mfn2
Tubulin
IP: HA
Mfn2
P-Tyr
D.
P-Tyr / Mfn2 (nomalized)
1.2
1.0
0.8
0.6
0.4
0.2
0
CTR
CSK-KD
*
E
CTR
c-Src-WT
c-Src-DN
IB:
Input
c-Src
Mfn2
Tubulin
IP: HA
P-Tyr
Mfn2
F.
P-Tyr / Mfn2 (nomalized)
3
2
1
0
*
*
CTR
c-Src-WT
c-Src-DN
G.
CTR
c-Src
CSK
Fyn
Lyn
Fgr
IB:
Input
HA
c-Src
CSK
Fyn
Lyn
Fgr
Tubulin
IP: HA
P-Tyr
HA
H.
P-Tyr / HA (normalized)
2
1
0
*
CTR
c-Src
CSK
Fyn
Lyn
Fgr
I.
Mfn2
Cytosol
OMM
Omi
IMS
OPA1
IMM
Matrix
CyD
J.
PK (-) (+)(+)(+)(+)(+) (+)(+)
Dig (-) (-).00 .04 .08 .12 .20 (-)
Triton X (-) (-)(-) (-)(-)(-) (-) (+)
c-Src
Mfn2
Omi
OPA1
CyD

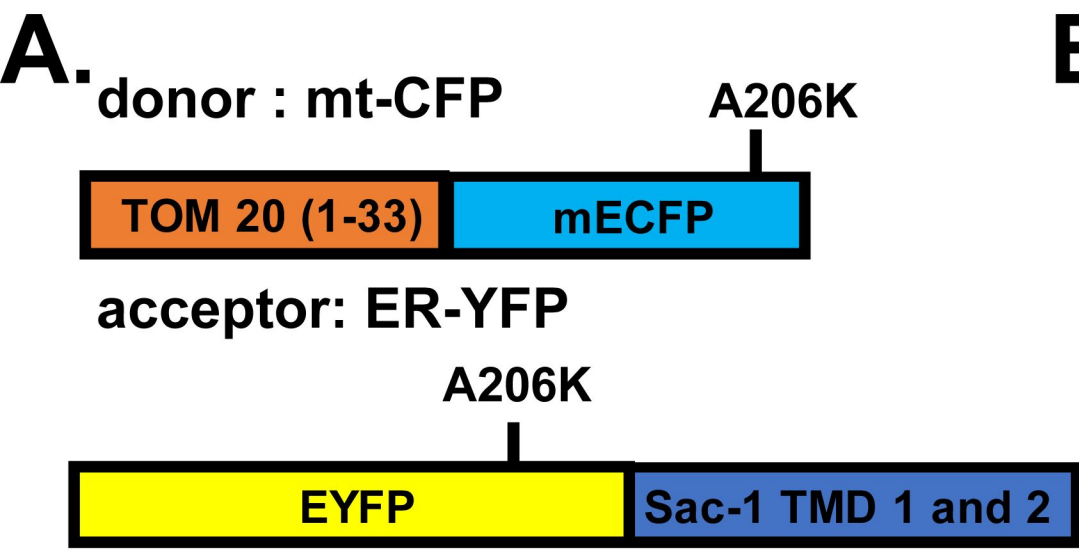

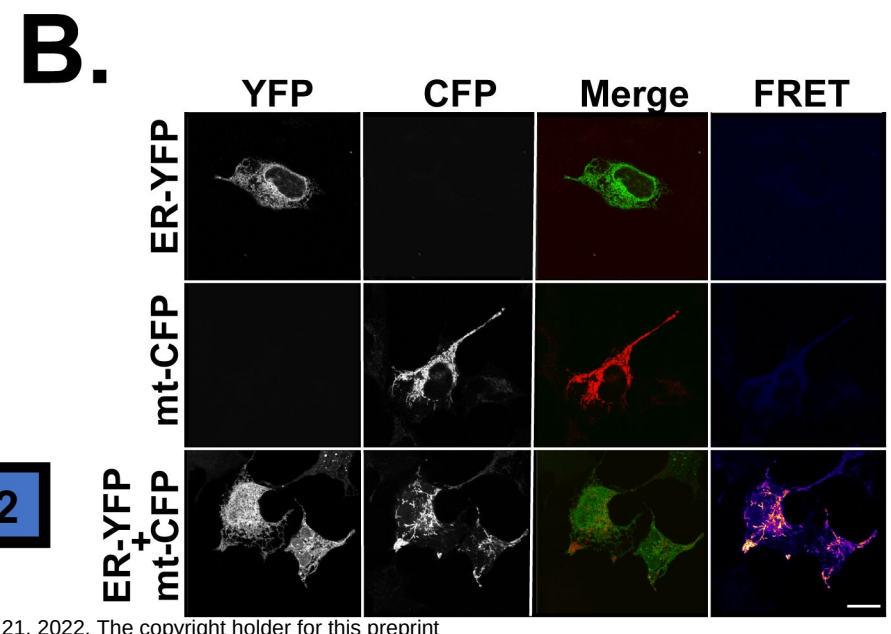

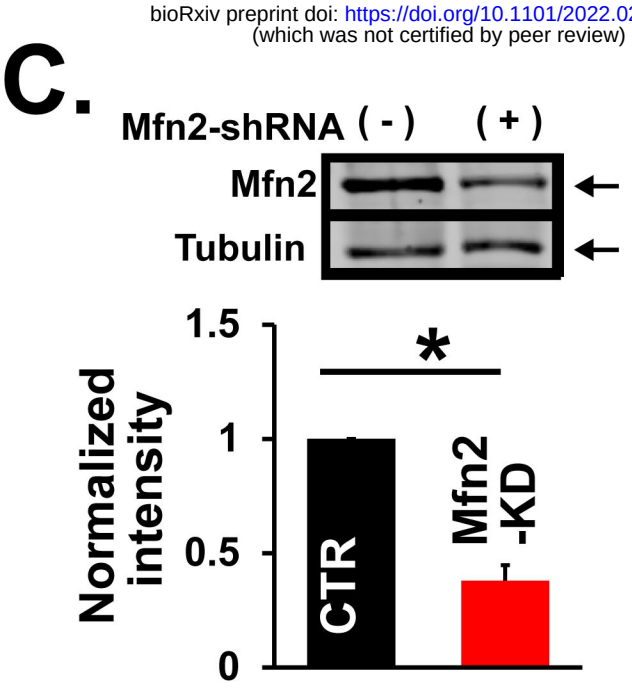

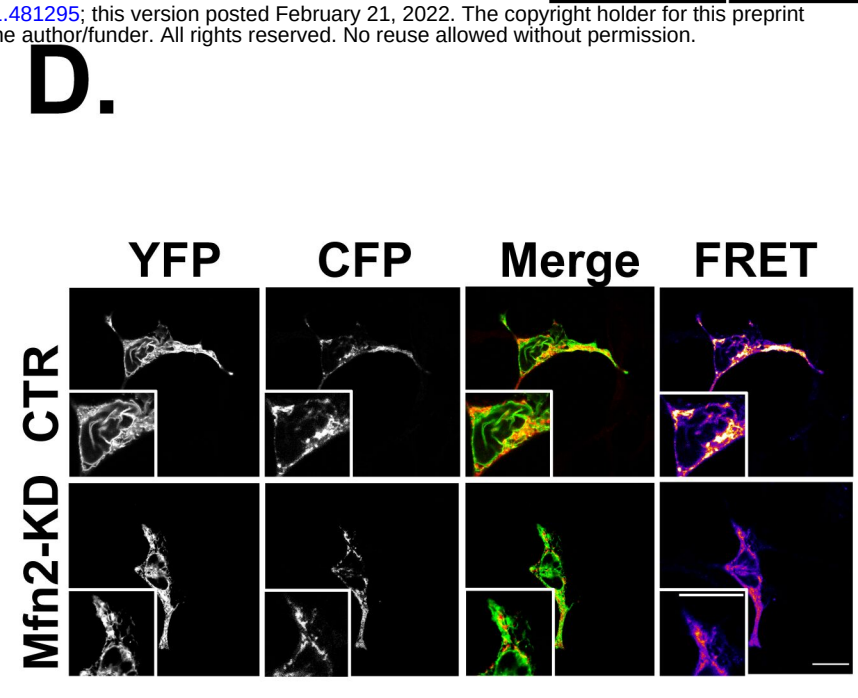

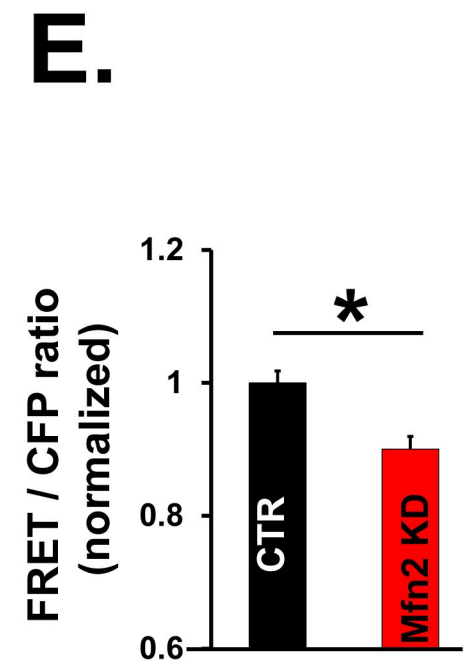

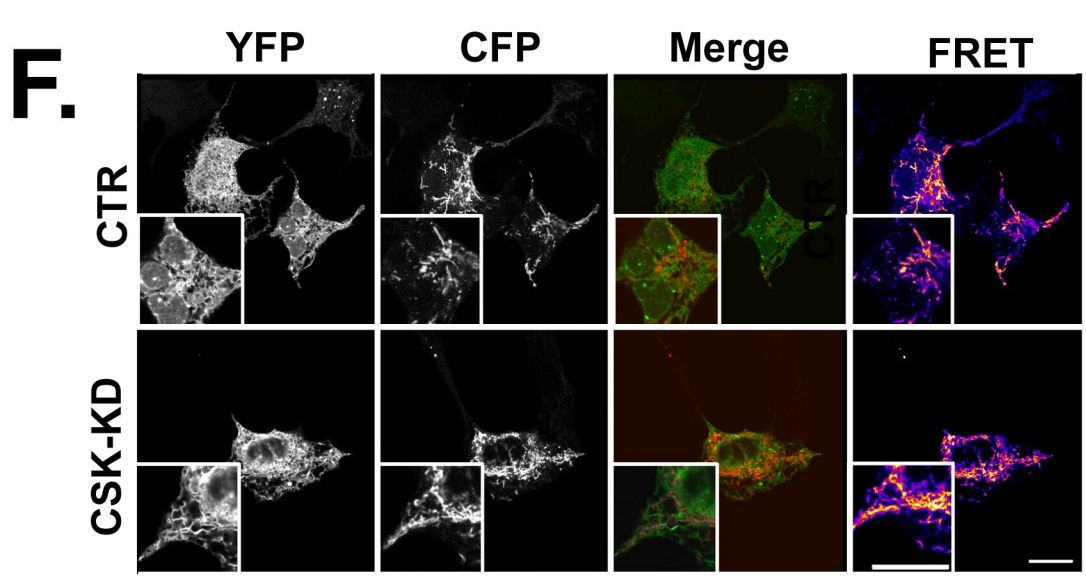

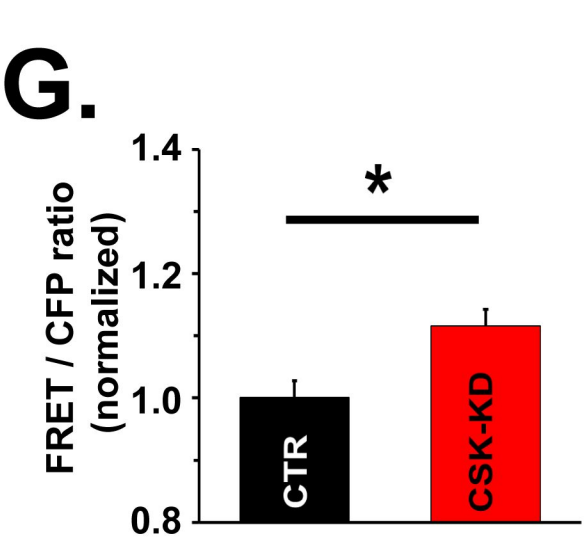

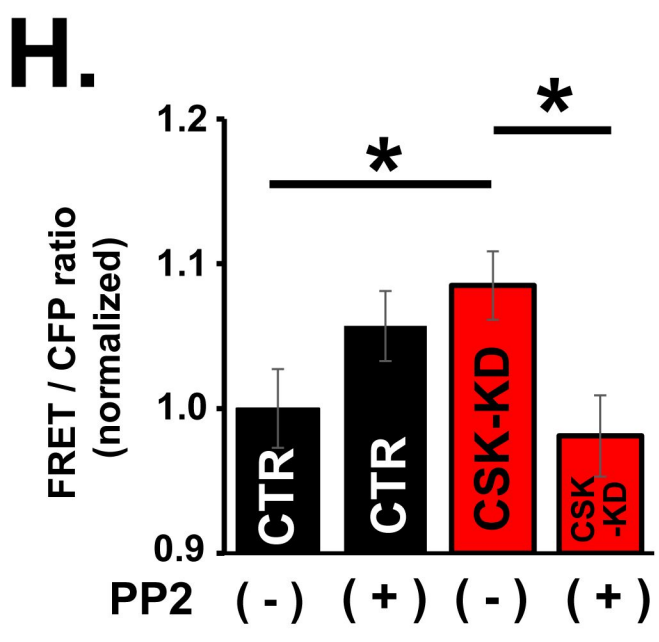

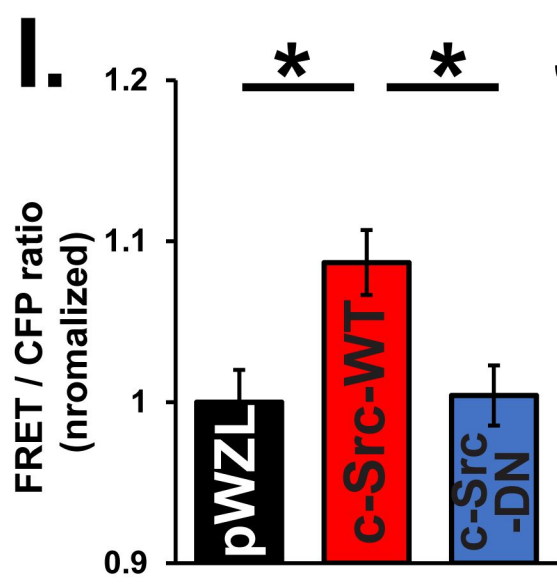

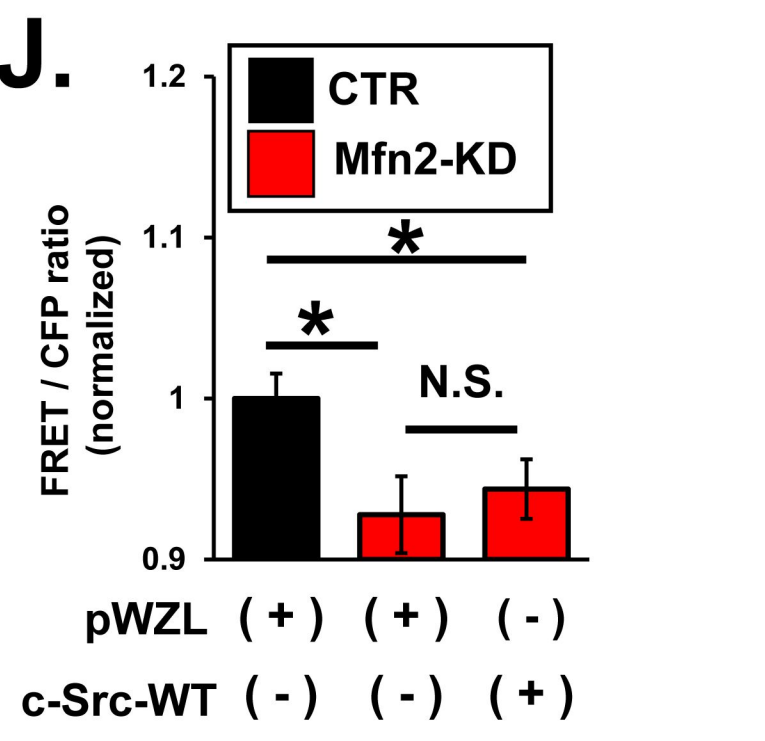

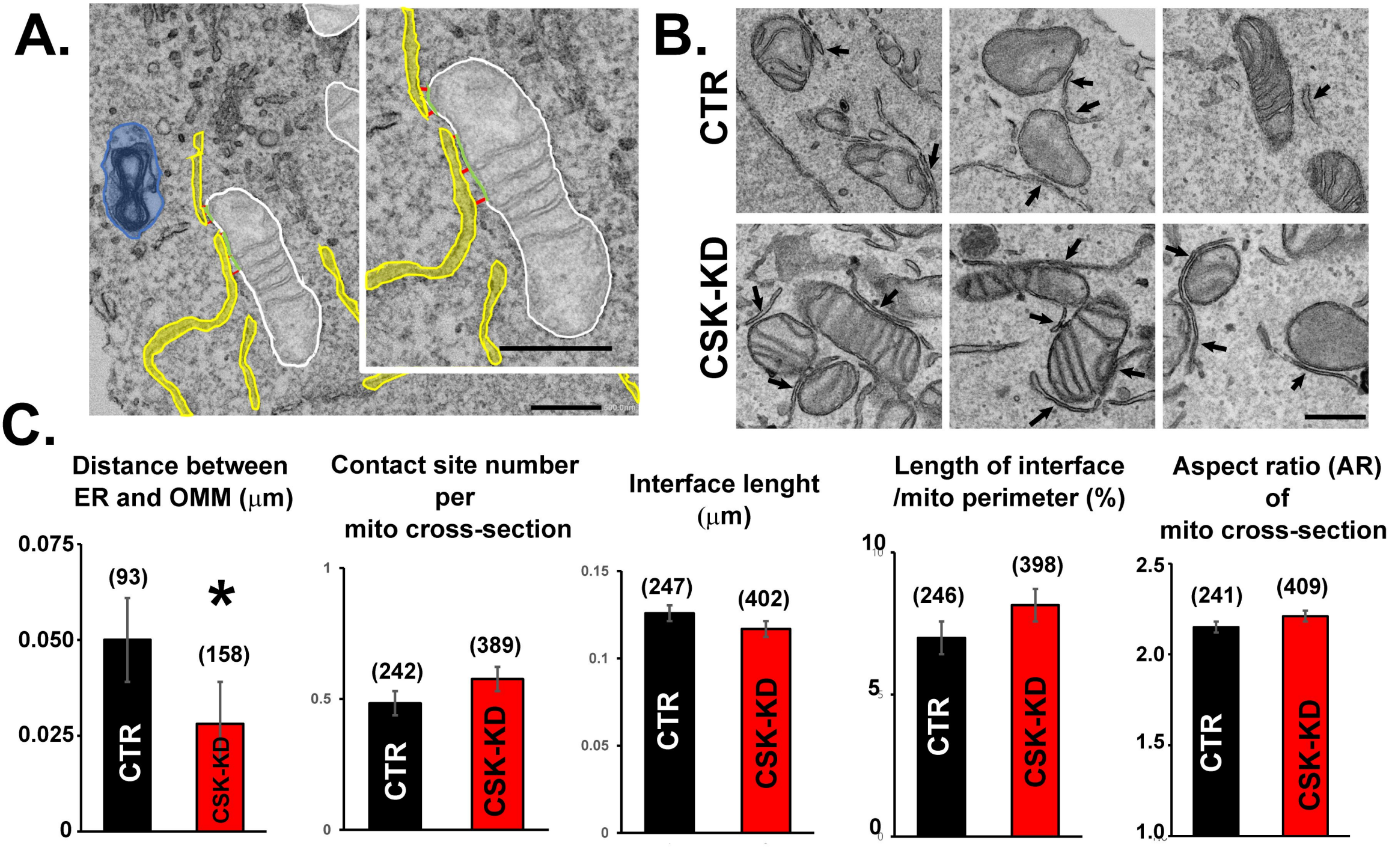
A.
B.
CTR
CSK-KD
C.
Distance between ER and OMM (μm)
0.075
0.050
0.025
0
(93)
(158)
*
CTR
CSK-KD
Contact site number per mito cross-section
1
0.5
0
(242)
(389)
CTR
CSK-KD
Interface lenght (μm)
0.15
0.1
0.05
0
(247)
(402)
CTR
CSK-KD
Length of interface /mito perimeter (%)
10
5
0
(246)
(398)
CTR
CSK-KD
Aspect ratio (AR) of mito cross-section
2.5
2.0
1.5
1.0
(241)
(409)
CTR
CSK-KD

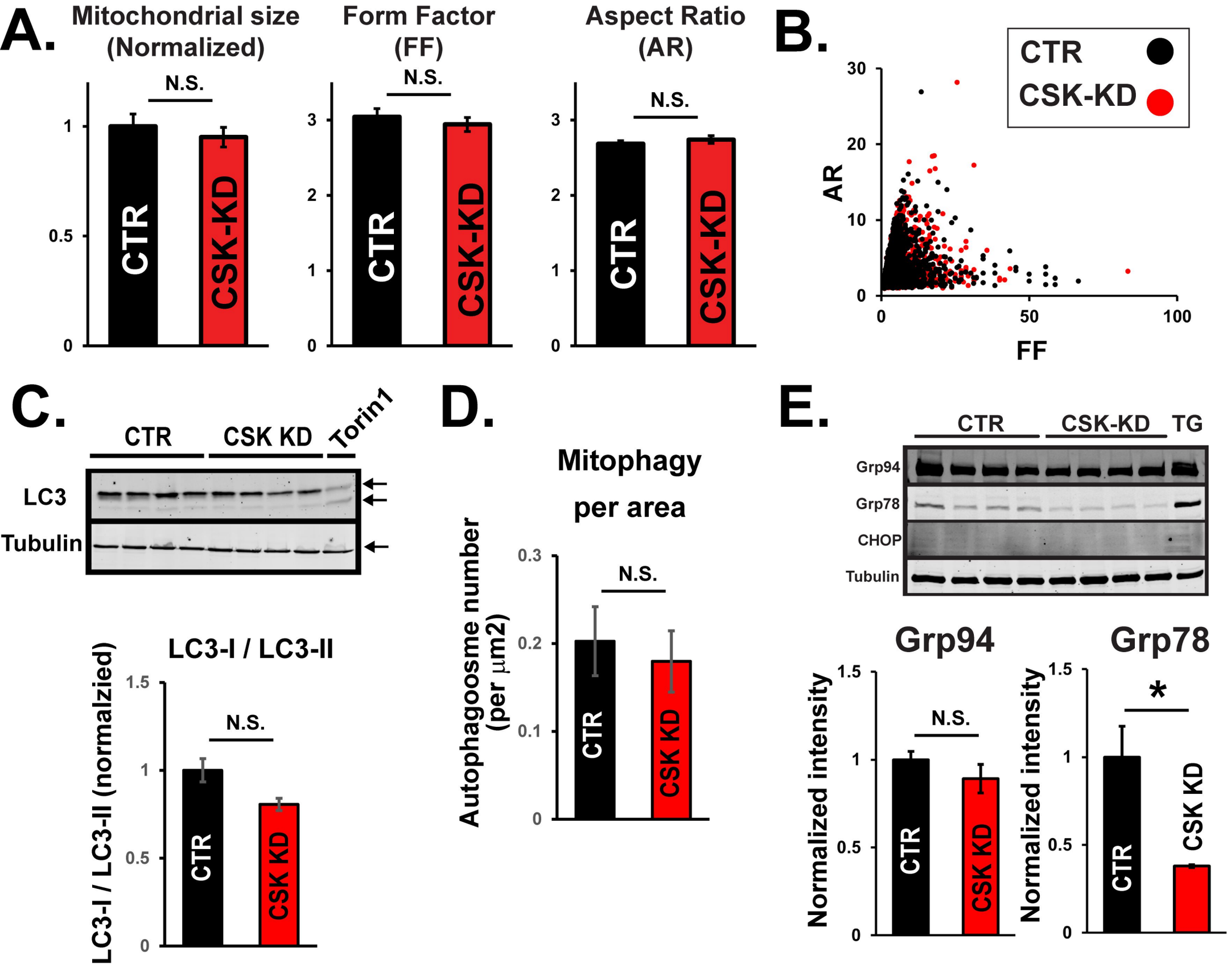
A.
Mitochondrial size (Normalized)
Form Factor (FF)
Aspect Ratio (AR)
N.S.
CTR
CSK-KD
B.
CTR
CSK-KD
AR
FF
C.
CTR
CSK KD
Torin1
LC3
Tubulin
LC3-I / LC3-II
LC3-I / LC3-II (normalzied)
CSK KD
D.
Mitophagy per area
Autophagoosme number (per μm2)
E.
CTR
CSK-KD
TG
Grp94
Grp78
CHOP
Tubulin
Normalized intensity
*

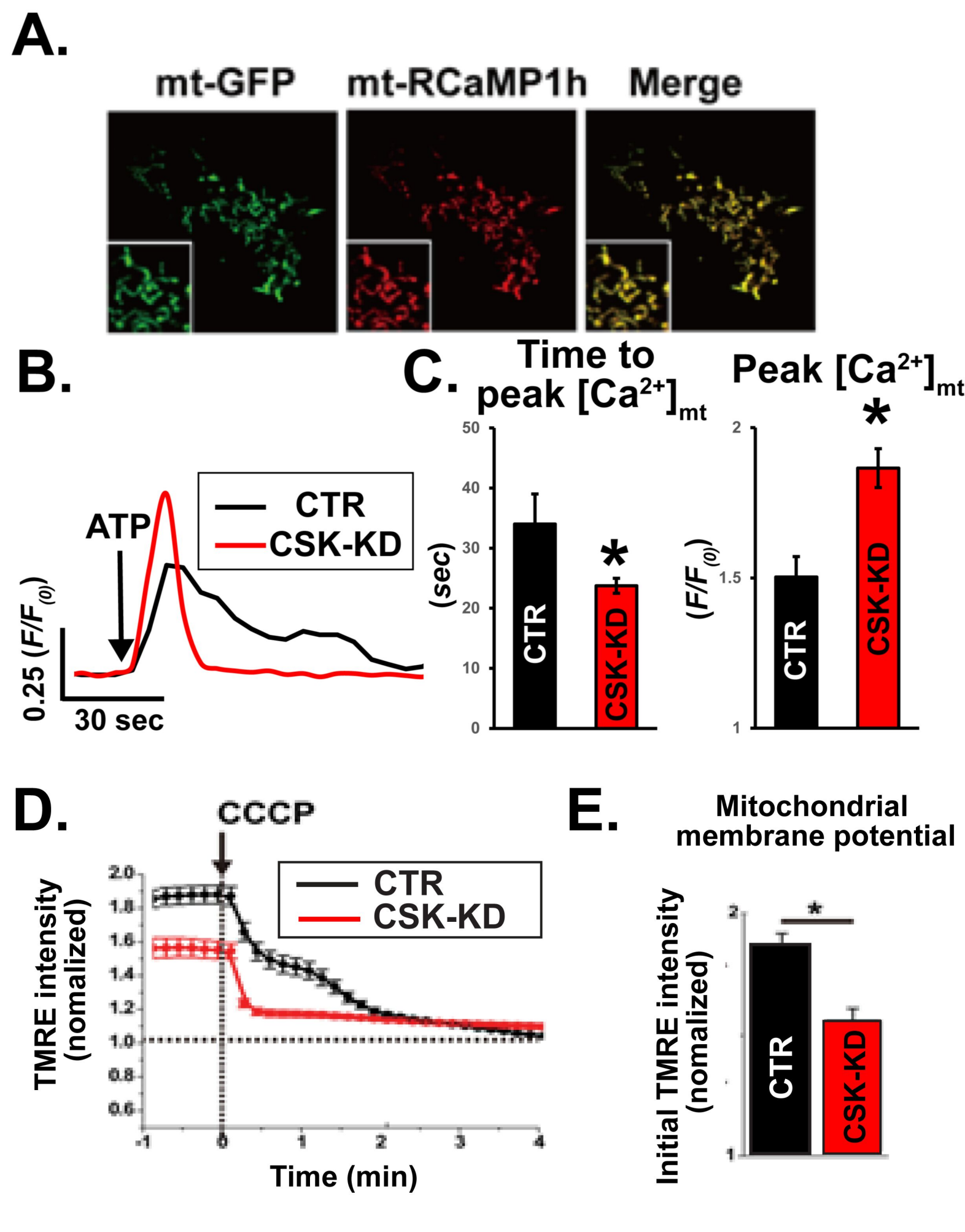
A.
mt-GFP
mt-RCaMP1h
Merge
B.
ATP
CTR
CSK-KD
0.25 (F/F(0))
30 sec
C.
Time to peak [Ca2+]mt
(sec)
50
40
30
20
10
0
CTR
CSK-KD
*
Peak [Ca2+]mt
(F/F(0))
2
1.5
1
CTR
CSK-KD
*
D.
CCCP
CTR
CSK-KD
TMRE intensity (nomalized)
2.0
1.8
1.6
1.4
1.2
1.0
0.8
0.6
-1
0
1
2
3
4
Time (min)
E.
Mitochondrial membrane potential
Initial TMRE intensity (nomalized)
2
1
*
CTR
CSK-KD